Wind Gates Search States in Free Flight

S. David Stupski[1] and Floris van Breugel[1]

[1]**Department of Mechanical Engineering, University of Nevada, Reno**

Corresponding author:
Floris van Breugel[1]

Email address: fvanbreugel@unr.edu

ABSTRACT

For any organism tracking a chemical cue to its source, the motion of its surrounding fluid provides crucial information for success. For both swimming and flying animals engaged in olfactory search, turning into the direction of oncoming wind or water current is often a critical first step [Marsh et al., 1978, Carton and Montgomery, 2003]. However, in nature, fluid flow may be turbulent or very still [Crall et al., 2017, Houle and van Breugel, 2023, Carvalho and Gonçalves, 2020], and it is unclear how organisms adjust their search strategies accordingly due to the challenges of separately controlling flow and chemical encounters. Here, we use the genetic toolkit of *Drosophila melanogaster*, a model organism for olfaction [Benton, 2022], to develop an optogenetic paradigm to deliver temporally precise "virtual" olfactory experiences in free-flying animals while independently manipulating the wind conditions. We show that in free flight, *Drosophila melanogaster* adopt distinct search routines that are gated by whether they are flying in laminar wind or in still air. We first confirm that in laminar wind flies turn upwind, and further, we show that they achieve this using a rapid ballistic turn. In still air, flies adopt remarkably stereotyped "sink and circle" search state characterized by $\sim 60°$ turns at 3-4 Hz, biased in a consistent direction. In both laminar wind and still air, immediately after odor onset, flies decelerate and often perform a rapid turn. Both maneuvers are consistent with predictions from recent control theoretic analyses for how insects may estimate properties of wind while in flight [van Breugel, 2021, van Breugel et al., 2022]. We suggest that flies may use their deceleration and "anemometric" turn as active sensing maneuvers to rapidly gauge properties of their wind environment before initiating a proximal or upwind search routine.

Keywords: Olfaction; Anemosensing; Sensory Integration; Search

INTRODUCTION

The ability to track a chemical cue to its source is critical for the fitness of motile organisms with diverse life histories. Bacteria with no brain navigate to the source of nutrients [Alon et al., 1999], benthic isopods track the smell of carrion on the dark ocean floor [McClain et al., 2019], and moths locate nectar-laden flowers in complex chemical landscapes [Riffell et al., 2014]. To succeed in tracking a plume to its source animals must contend with cues that are intermittently dispersed in space by natural advection processes [Moore and Crimaldi, 2004]. Over a century of research [Barrows, 1907, Baker et al., 2018] has provided a clear picture of how animals track plumes in consistent laminar flow. A nearly ubiquitous strategy is to adopt a stereotyped "cast and surge" behavior; surging into the direction of flow upon encountering a chemical plume and performing cross flow, casting counter turns after losing track of the plume [Marsh et al., 1978, van Breugel and Dickinson, 2014, Carton and Montgomery, 2003, Nevitt et al., 2008, Grasso and Basil, 2002]. Cast and surge has served as the scaffolding for ethological, robotic, and algorithmic studies of plume tracking spanning since the turn of the 20th century [Singh et al., 2023, Barrows, 1907].

In nature however, the air or water surrounding an organism is rarely consistent, and can be very still or turbulent [Crall et al., 2017, Houle and van Breugel, 2023, Carvalho and Gonçalves, 2020]. How then should a flying organism track a plume when ambient flow is below detection thresholds? Prior studies have suggested that flies do adopt qualitatively different strategies in windy vs. quiescent conditions [Saxena et al., 2018]. However, discovering the behavioral mechanisms underlying olfactory navigation in still air has been nearly impossible because even in still air, an odor source can generate a spatiotemporally complex 3-D plume structure [Connor et al., 2018] . It would then be indistinguishable which elements of search change because of the wind environment and which elements of search have changed due to differences in encounter dynamics with the plume itself; another critical component of plume tracking [Kadakia et al., 2022]. Because of the difficulty in knowing the precise locations of plumes, and their dispersal within space changing based on the wind environment, it is not surprising that our understanding of how organisms modulate their plume tracking in still air is lacking.

Here we characterize olfactory search in still air by developing an optogenetic paradigm to deliver a spatiotemporally precise fictive odor experience to freely flying *Drosophila*, an established model system for olfaction [Benton, 2022]. We accomplish this by combining real-time 3-D tracking of flying flies with optogenetic control of olfactory receptor neurons (ORNs), following the recent success of applying this tool to remotely activate ORNs using red light in walking flies [Kadakia et al., 2022, Matheson et al., 2022, Tao et al., 2023]. We first robustly demonstrate that the fictive odor experience elicits the same stereotypical olfaction driven search behaviors that flying *Drosophila* exhibit in laminar wind after detecting an appetitive odor. We then use this approach to answer a simple, but otherwise experimentally intractable question: what does a flying fly do if it detects an odor and there is no wind to surge into? In still air, flies adopt a previously undescribed, highly stereotyped search behavior characterized by a sequence of rapid turns in a consistent direction while also lowering their altitude. This ”sink and circle” style of plume tracking is the still air complement to the well described ”cast and surge” routine that flies perform in the presence of laminar wind. Furthermore, we reveal a previously overlooked aspect of the cast and surge strategy in Drosophila. Flies surge into the wind using a rapid ($\sim$100 ms) turn that exhibits similar kinematics to ballistic turns referred to as saccades (in analogy with rapid eye movements of primates [Collett and Land, 1975]).

Our discovery of sink and circle, and the ballistic upwind turn, indicates that flies can both estimate the presence and direction of ambient wind while flying. However, without access to stationary sensors, or magnitude calibrated sensory systems, a flying insect cannot directly measure information about the wind environment [Schone, 2014, van Breugel, 2021]. Instead, they perceive apparent wind, the vector sum of and ambient wind and relative airflow due to self motion. Historically, wind orientation in insect flight has been attributed to visual anemotaxis [Kennedy et al., 1940, Kennedy and Marsh, 1974]: a wind orienting strategy that uses angular measurements of ventral optic flow and the apparent wind direction to guide an insect into the direction of ambient wind. The only stable solution to a control strategy that minimizes the difference between these two angles is to orient upwind [van Breugel et al., 2022]. Visual anemotaxis, however, would not allow a fly to distinguish between flying upwind or flying in still air, nor would it explain how a fly can perform a directed saccade into the direction of ambient wind, or maintain a crosswind casting course. Our results indicate that flying *Drosophila* do not rely on visual anemotaxis to turn into the wind. Instead, our data offer support to an alternative hypothesis [van Breugel et al., 2022]: that flies use an active sensing maneuver consisting of decelerating and a rapid change in course at the onset of an odor event to gauge properties of the wind.

RESULTS

Activating Orco+ Neurons in flight generates stereotypical cast and surge behaviors

To independently control the wind and olfactory experience of flying flies we developed a custom-built wind tunnel capable of delivering 40 cm/s laminar wind or still air (Figure 1A). The tunnel was equipped with machine vision cameras to track flies in 3-D at 100 Hz against uniform infrared illumination, while flies were provided with a combination of blue and white illumination (425 lux total) so they could navigate the space. When a fly entered a pre-defined “trigger zone” (Figure 1B) it was assigned either a “flash” condition which turned on two symmetric rows of red LEDs for 625 ms, or a “sham” corresponding to no light flash (Figure 1B). The average intensity of the red light in the trigger zone was 42 μ W mm^{-2} (Supplemental Figure 2).

Optogenetic activation of *Orco*+ neurons generated a strong anemotaxis response (Figure 1C-D) within 310 ms (compared to previous sensorimotor delays of 200 ms [van Breugel and Dickinson, 2014]), with maximally, 92% of trajectories adopting an upwind course direction (mean course error from upwind of 15.7° $\pm$ 24.5 °, Figure 1D). In contrast, we did not find evidence of anemotaxis in sham controls for Orco>CsChrimson flies, flash and sham conditions for wild-type flies (Figure 1C-D), or for a genetic control (UAS-CsChrimson/+, Supplemental Figure 3). There was however, a barely detectable and time delayed anemotaxis response in Orco>CsChrimson flies raised without supplemental ATR (Supplemental Figure 3).

Approximately 540 ms after the optogenetic stimulus ended, the course direction of Orco>CsChrimson flies was largely perpendicular to the wind direction, characteristic of the casting behaviors observed for insects interacting with a real odor plume [van Breugel and Dickinson, 2014] [Dekker and Cardé, 2011]. These response times are comparable to the 450 ms delay seen in casting initiation after losing contact with a real ethanol plume [van Breugel and Dickinson, 2014]. We did not see any evidence of casting as a result of the red light flash in any genetic or positional controls (Figure 1D, Supplemental Figure 3).

Orco>CsChrimson flies displayed a significant deceleration effect in response to optogenetic stimulation compared to sham trials (Figure 1E, Mann-Whitney U test, p=5x10^{-3}). We found no evidence of this effect in wild-type, or genetic controls, suggesting that it was not a visually mediated startle re-

sponses. Although this deceleration behavior was not originally reported, our re-analysis of flies tracking a well-defined ethanol plume revealed a similar, albeit more subtle, deceleration effect (Supplemental Figure 3). Decelerating in response to encountering an odor has also been reported for flies elsewhere [Saxena et al., 2018]. Orco>CsChrimson flies also reduced their altitude in response to optogenetic activation of *Orco+* neurons 240 ms after a triggering event (Figure 1F, Mann-Whitney U test, p=5.8 x10^{-3}) and continued to maintain a lower altitude throughout the entire time course. The altitude difference levelled out at around 19 cm within 2 seconds of flies entering the trigger zone. Initially we hypothesized that the altitude lowering may have been due to attraction to the visually salient optic flow grid. However, when we performed the same experiment without a visual checkerboard on the wind tunnel floor, flies still reduced their altitude in response to optogenetic activation of *Orco+* neurons (Supplemental Figure 4). We did not find any noteworthy altitude modulation effects in wild-type flies, or any genetic controls in response to a flash of red light.

Optogenetic Activation of *Orco+* Neurons Elicits Search for Visually Contrastive Features

Activating *Orco+* neurons in flight also evoked visually guided search in *Drosophila* similar to published free flight experiments performed with ethanol, vinegar, and CO_2 plumes [van Breugel and Dickinson, 2014, van Breugel et al., 2018]. We first reciprocated visually evoked search behaviors in our wind tunnel, using an ethanol plume and a 3.8 cm diameter, dark, infrared transmissive, acrylic disc, 35 cm downwind of the odor source. We quantified the probability that a trajectory from wild-type flies approached the object both in the presence and absence of the ethanol plume (Figure 1G). We considered a trajectory to have approached the object if it entered a 10 cm radius around the acrylic disc (Figure 1H). Even though there was no red light triggering in our wild-type experiments we only included trajectories from flies which entered the trigger zone volume of the tunnel. Consistent with prior work [van Breugel and Dickinson, 2014], we found that flies were approximately 50% more likely to enter the airspace around the dark visual feature in the presence of an ethanol plume (Figure 1I, two-proportion Z-test, p=2.8x10^{-7}). Next we used the same optogenetic activation paradigm described in the previous section, only this time with the same dark visual feature used in our ethanol plume experiments. We focused our analysis on the first 5 seconds after a trajectory initiated a triggering event. Orco>CsChrimson trajectories that received a flash of red light approached the object 51.5% of the time, more than twice that when compared to the trajectories assigned a sham event (Figure 1I, two-proportion Z-Test, p = 3.6x10^{-23}). Orco>CsChrimson trajectories from sham events and wild-type flies flying in clean air had similar levels of attraction to the object Figure 1I, (two-proportion Z-test, p=.14), suggesting that only a very recent experience with an odor elicits visual approach.

Flies change search states in still air

After establishing that our optogenetic approach elicits the full suite of established olfactory navigation behaviors for flies flying in laminar wind, we set out to answer a question that would not be feasible using a real odor. How do flies modulate their search behavior depending on their wind environment? Whereas the the first few hundred ms after the onset of the olfactory stimulus was similar regardless of whether or not flies were flying in wind or still air, after the stimulus ended trajectories displayed a strikingly different, and highly stereotyped search behavior. Rather than surging and casting, flies in still air performed a sequence of rhythmic uni-directional turns resulting in a tight circling behavior centered around the point where the optogenetic stimulus ended (Figure 2A-B). Flies did not orient into any particular part of the wind tunnel (Figure 2C). However, similar to activation of *Orco+* neurons in wind, flies also sharply decelerated on the stimulus onset (Figure 2D). We did not robustly observe this behavior, or any other artifacts, in either the sham trajectories for Orco>CsChrimson flies or any wild-type controls (Supplemental Figure 5). The circling behavior consisted of two primary motifs: sharp, regular saccades in a consistent direction, while also reducing altitude.

Circling is Characterized by Turns with Stereotyped Amplitude, Frequency, and Directional Bias

Fruit flies typically change course via rapid turns referred to as saccades in the literature [Collett and Land, 1975]. To quantify the stark differences in post-stimulus saccade dynamics in laminar wind vs. still air, we adapted and slightly modified the Geometric Saccade Detection algorithm originally found in [Censi et al., 2013] (Figure 3A, Supplemental Figure 1) and characterized properties of saccades identified from 0.9-3 s after the stimulus. This allowed us to compare saccades specifically from circling and casting behaviors.

In still air, Orco>CsChrimson flies' post-stimulus circling saccades were remarkably consistent in amplitude, following a unimodal distribution around 60°(Figure 3B, mean =59.1 deg +/- 31.2). In contrast, Orco>CsChrimson flies engaged in post flash casting had a long tailed distribution of saccade amplitudes, mixed between frequent small saccades and less frequent large amplitude ones. The amplitudes of saccades from Orco>CsChrimson flies which received a sham triggers in still air, wild-type flies in laminar wind

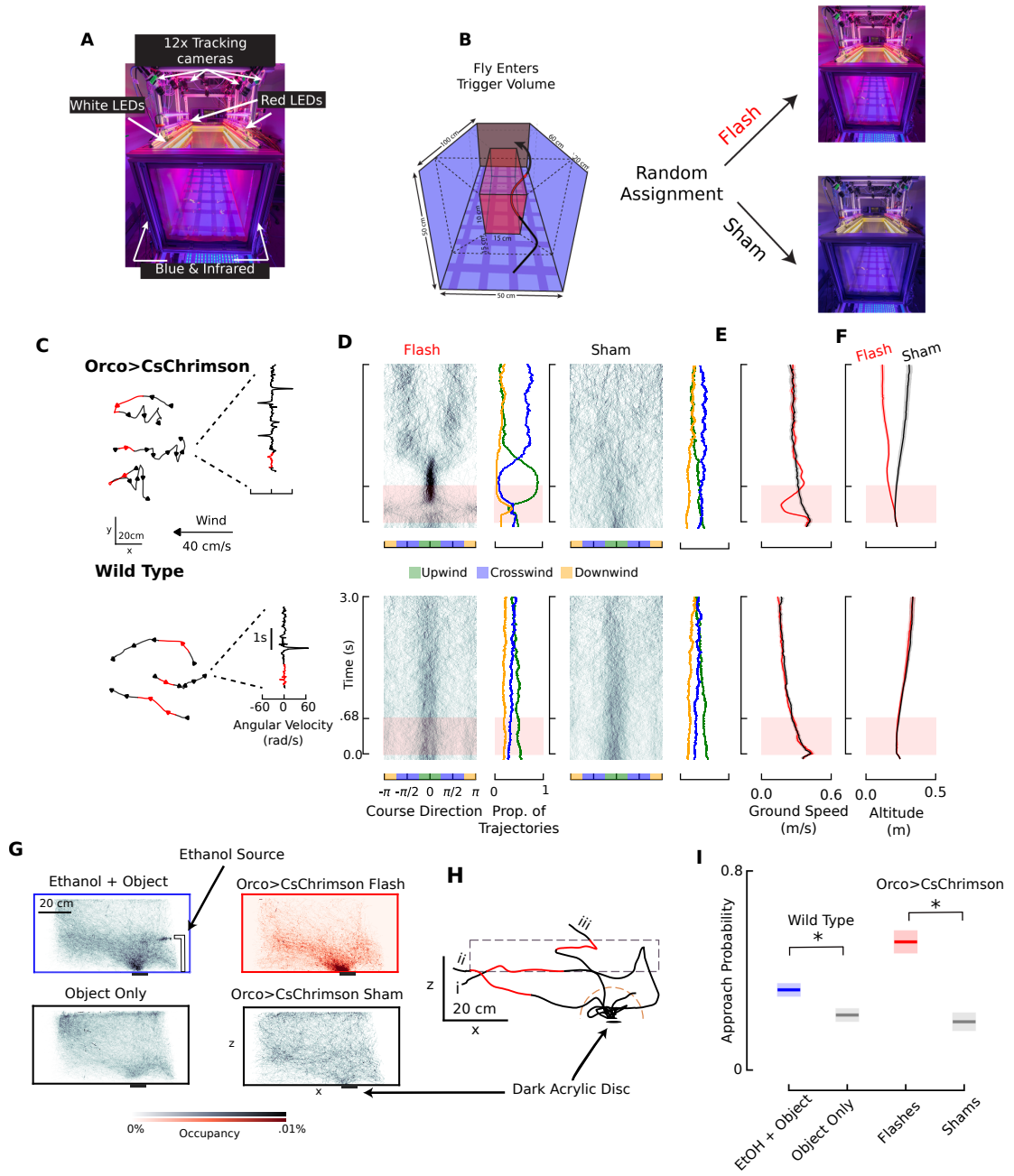

Figure 1. Reciprocation of stereotyped plume-tracking responses using optogenetics. **A)** Wind tunnel system for free-flight optogenetics. **B)** Experimental design: a trajectory enters the trigger zone and is randomly assigned a "flash" or "sham" event. **C)** Three sample trajectories in the x, y plane of Orco>CsChrimson flies and wild-type flies and their response to a 675 ms flash of red light. Red regions indicate the portions of trajectories during which the 675 ms flash was activated. **D)** Course direction vs time relative to the trajectory entering the trigger zone for Orco>CsChrimson flies (top) and wild type flies (bottom) that received either a flash stimulus or a sham event (Orco>CsChrimson flash, n=232 trajectories; Orco>CsChrimson, sham n=222 trajectories; wild type, flash n=398 trajectories; wild type, sham n= 429 trajectories). A course direction of 0 indicates upwind and π/-π is downwind. Next to each course direction heat map is the fraction of trajectories oriented upwind (green), crosswind (blue) or downwind (orange). **E)** Ground speed response of Orco>CsChrimson and wild-type flies in response to a red light stimulus (red trace) compared to shams (black trace). **F)** Same as **E** except for altitude responses from optogenetic stimulus. **G)** Heat maps in the x, z plane of trajectory occupancies within the wind tunnel volume with a dark feature on the tunnel floor. **H)** Three example trajectories of Orco> CsChrimson flies entering the trigger zone (dashed rectangle), receiving a stimulus, and entering the airspace above the object (dashed semicircle). **I)** Object approach probability based on experimental conditions: Wild-type flies with an ethanol plume, n=1169; wild-type flies in clean air, n=856; Orco>CsChrimson trajectories randomly assigned a flash event, n=445; Orco>CsChrimson sham events, n=435. Shading in panels E, F, and I, and through the manuscript, indicates 95% confidence intervals.

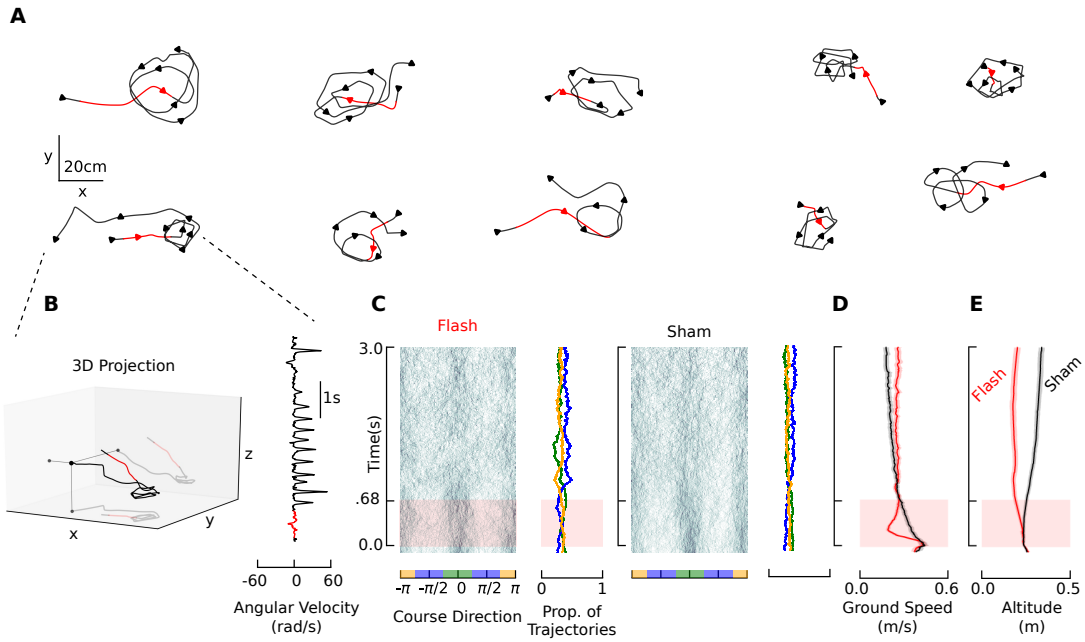

Figure 2. Optogenetic activation of OSN's in still air elicits circling rather than casting. **A)** Ten sample trajectories of the search behaviors of Orco>CsChrimson flies following optogenetic stimulation of *Orco+* neurons in still air. **B)** Sample 3D projection and angular velocity profile of a trajectory. **C)** Course direction in the same reference frame as Figure 1D for flash (n=263 trajectories) and sham (n=291 trajectories) conditions. **D)** Ground speed changes in response to activating of *Orco+* neurons in the absence of wind. **E)** Altitude responses of Orco>CsChrimson flies in response to an optogenetic stimulus in the absence of wind.

and wild-type flies in still air all had similar long-tailed distributions, although casting flies used larger amplitude saccades more frequently (Figure 3B).

In addition to changes in the distribution of saccade amplitudes, Orco>CsChrimson flies which received a flash event in still air had a higher saccade frequency than those either casting in laminar wind (still air, flash: 3.4 $\pm$.95 Hz; laminar wind, flash: 2.9 $\pm$.96 Hz) (Figure 3C). Orco>CsChrimson trajectories which were assigned sham events had similar saccade frequencies regardless of whether or not they were in still air or laminar wind (still air, sham: 2.5 $\pm$1.0 Hz; laminar wind, sham: 2.4 $\pm$1.0 Hz). Wild-type flies had lower saccade frequencies than Orco>CsChrimson flies, including Orco>CsChrimson flies which received sham events. We attribute this as likely being due to the history of Orco>CsChrimson flies having olfaction experiences throughout the night changing their baseline behavior, whereas wild-type flies do not. Wild-type flies typically had similar saccade frequencies regardless of which trigger event they received, and whether or not they were flying in laminar wind or still air (still air, flash: 1.9 $\pm$1.0 Hz; laminar wind, flash: 1.9 $\pm$1.1 Hz; still air, sham: 1.8 $\pm$.95 Hz; laminar wind, sham: 2.1 $\pm$ 1.2 Hz). Although there were technically statistically significant differences among these conditions, effect sizes were unnoteworthy (Figure 3C).

In still air, post stimulus saccade dynamics became directionally consistent. Flies were nearly 3 times as likely to perform a saccade in the same direction as their prior saccade as opposed to the other direction (Figure 3D). This was significantly more ipsilaterally biased than any other condition (Z-test of proportions, p=$9.3\text{x}10^{-38}$) . All other experimental conditions were either not ipsilaterally biased, or were biased drastically less so (Figure 3D). We found no obvious causality for whether a trajectory adopted a clockwise or counterclockwise bias.

Circling is specifically in response to the loss of an odor

We next asked if circling in still air was triggered specifically by the loss of the odor stimulus by implementing a "double flash" experiment. In these experiments, flies received either two 675 ms light flashes 1 second apart, or two shams (Figure 4A-B). We restricted our analysis to trajectories that extended for the full 3.4 seconds after the first stimulus. We pooled sham trajectories from the single and double flash experiments with the single flash experiments described earlier to make up for the fact that many sham trajectories were shorter than 3.4 seconds.

Sham trajectories showed no significant changes in mean angular velocity over the 3.4 seconds we

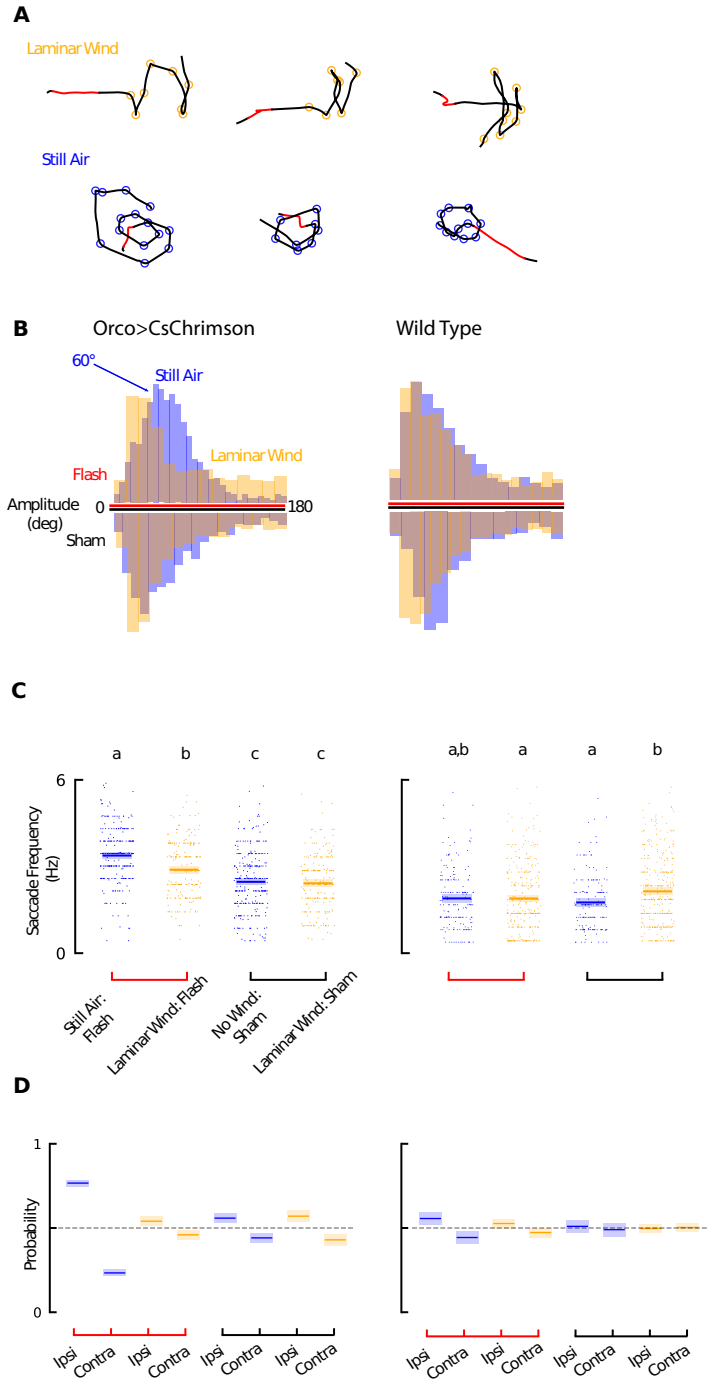

Figure 3. Saccade dynamics after optogenetic stimulus change in amplitude, frequency and directional consistency based on the wind environment. **A)** Six example trajectories of Orco>CsChrimson flies from either casting or circling conditions and where the mGSD algorithm annotated saccades (orange circles from laminar wind trajectories, blue circles from still air trajectories). **B)** Saccade amplitude distributions from Orco>CsChrimson flies (left) in laminar wind (orange n=1230 flash, n=922, sham) or still air (blue n=1930 flash saccades; sham, n=1459). Distributions above the axis indicate trajectories from a flash event, and distributions below the axes indicate data from sham assignments. Wild-type controls are on the right hand side of the figure for **B-D** (laminar wind flash saccades, n=1134; laminar wind sham, n=1344; still air flash, n=695; still air sham n=648). **C)** Saccade frequencies of trajectories from laminar wind or still air and their associated sham controls. Letters indicate statistical groupings within a genotype (Mann-Whitney U test with Bonferroni Corrected α = .0083). **D)** Ipsilateral vs. contralateral bias of saccades for each wind, flash, and genotype condition.

analyzed. Flies receiving a single flash showed a sharp increase in mean angular velocity immediately after when the stimulus ended (Figure 4B-C). Their angular velocity remained elevated for 2 seconds before tapering off slightly (Figure 4B-C). When flies received a second flash, they reduced their angular velocity during the stimulus, and subsequently re-initiated circling when the second flash ended (Figure 4B-C). We found no evidence of a visually mediated response to light flashes in wild-type controls (Supplemental Figure 6).

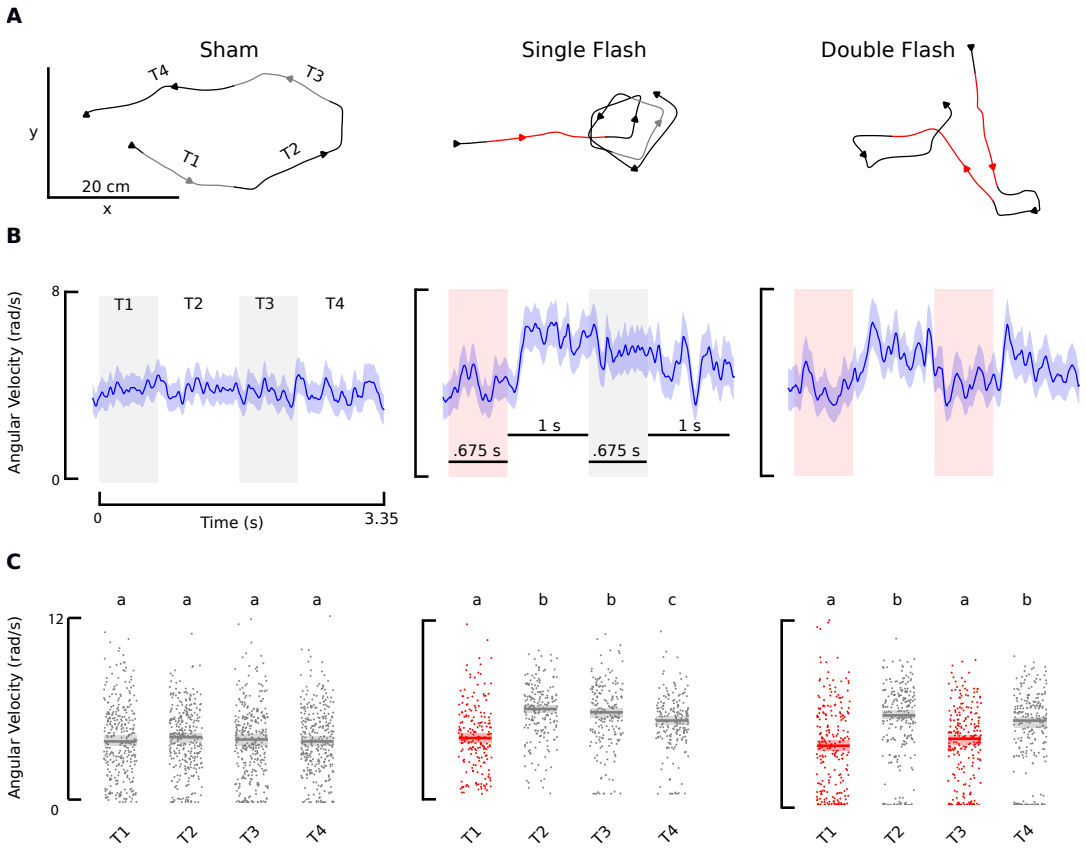

Figure 4. Circling is a response to odor loss. **A)** 3.4 second sample trajectories in the x, y plane of flies that received no optogenetic stimulus, a single red light flash stimulus, or two flashes separated by one second. Red color indicates the portion of the trajectories during which the red light stimulus was active and gray indicates the portion of the trajectories which are temporally aligned with the optogenetic stimulus of the two flash experiment, but did not receive a red light stimulus during that time. **B)** Mean population angular velocity responses for the respective no flash (n=316 trajectories), single flash (n= 200 trajectories), and double flash (n=241 trajectories). **C)** Mean angular velocities of individual trajectories over each of the four time regions of interest during their flight relative to entering the trigger zone: the first 675 ms (*T1*) the following intermittent second (*T2*), a secondary 675 ms portion (*T3*), and the subsequent one second period (*T4*). Letters represent statistical groupings that can be compared within a stimulus regimen. Statistical groupings were determined by Mann-Whitney U tests with a Bonferroni corrected α of .0083.

Search in still air is a proximal search strategy

We hypothesized that the behavior flies use in still air is likely a proximal search strategy. To show this visually, we aligned each trajectory in the horizontal plane around the point at which the fictive odor ended (Figure 5A-B). In still air, Orco>CsChrimson flies which received an optogenetic stimulus stayed significantly closer to the point at which the odor was lost compared to Orco>CsChrimson flies in laminar wind (Figure 5C). This difference was greatest 1.1s after the end of the optogenetic stimulus; in still air flies stayed on average 10 cm closer to the point of odor loss compared to flies in laminar wind, the maximum difference was only 3.5 cm when comparing sham trajectories from both wind conditions. Wild-type flies did not travel as far in still air as in laminar wind, however this was explained by differences in

ground speeds in the two wind conditions. The flash events had no effect on the distance they travelled (Supplemental Figure 7).

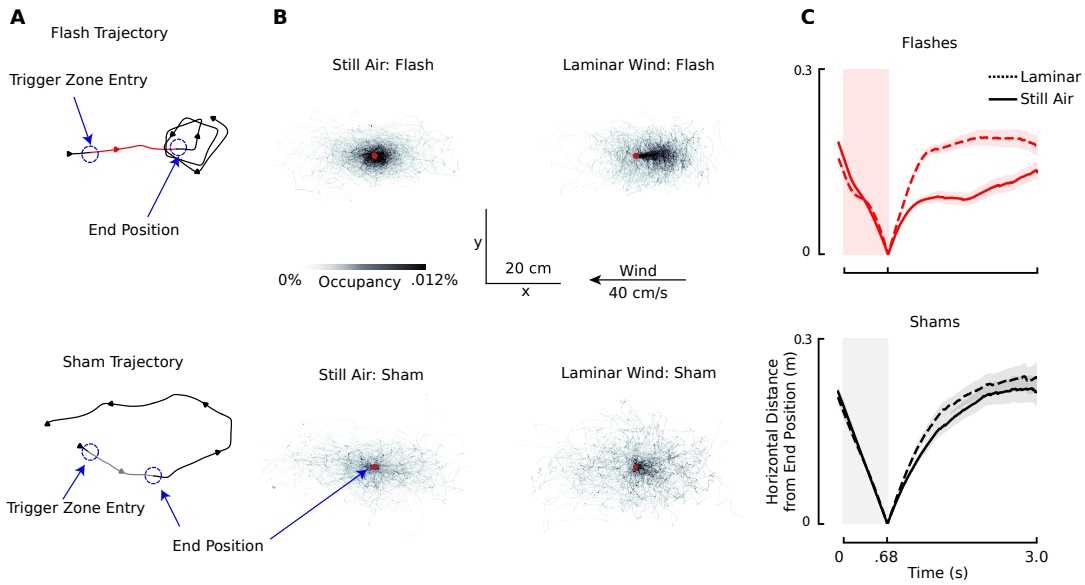

Figure 5. Search in still air is a proximal search strategy. **A)** Example trajectories from flies that received a flash (top) or sham (bottom) assignment. Red indicates portions of the trajectory during which the red light stimulus was active and gray indicates the 675 ms region after the sham trajectory entered the trigger zone. **B)** Heat maps of trajectories with origin set to the flies position 675 ms after entering the trigger zone (i.e. when the stimulus turned off for flash events). Heat maps exclude the portions of the trajectories up until 675 ms after entering the trigger zone. Orange dots indicate the point of alignment for all trajectories. **C)** Mean horizontal distance from the end position for Orco>CsChrimson flies which received either a flash (top) (laminar wind: n=232 trajectories; still air: n=263 trajectories) or sham (bottom) (laminar wind:n=222 trajectories; still air: n= 291 trajectories) assignment. Dashed lines are the population mean of flies from laminar wind experiments and solid lines represent flies from still air experiments.

Anemotaxis is often a ballistic, two-turn sequence

While the existence of wind gated search strategies suggests flies can estimate wind magnitude while flying, it is less obvious how they might do so. We suspect that flies estimate properties of the wind in the first few hundred milliseconds after activation of OSN's, during which time the behavior of flies is remarkably similar despite flying in still air or laminar wind. We found that in both laminar wind and still air, activating *Orco+* neurons caused flies to decelerate (Figure 6A). For a fly flying in laminar wind, this deceleration event was coupled with a sharp change in course direction. Flies flying in still air had a much more subtle course change response (Figure 6A). Neither wild-type flies nor genetic controls exhibited a deceleration or change in course in response to the red light flash (Figure 6A, Supplemental Figure 8), indicating that both maneuvers are likely olfactory responses. In laminar wind, anemotaxis itself was a second sharp turn which directly followed the initial course change, manifesting as a sequence of two rapid turns (Figure 6B).

The two-turn anemotaxis sequence was most stereotyped in flies broadly oriented upwind at the time of the stimulus (Figure 6C). More than half of crosswind oriented flies also used a two-turn sequence to perform anemotaxiseven often passing through an upwind heading during the initial turn before correcting with a second (Figure 6B-C). Flies oriented downwind at the time of the stimulus did not display stereotyped wind orienting behavior (n=26 total trajectories, Supplemental Figure 8) and were not included in this analysis. The magnitude of the initial turn tended to be larger for flies oriented more upwind at the time of the stimulus (Figure 6D). Although not visually mediated we cannot entirely rule out that this behavior may be linked to the somewhat unnatural odor experience of activating all *Orco+* neurons simultaneously. However, we also find evidence that flies perform a similar two-turn sequence upon entering an ethanol plume using previously published data (Supplemental Figure 9), suggesting that this is a critical but previously overlooked component of olfactory navigation in flies.

We next asked if the two turns are body saccades, which are thought to be feed-forward motor programs for flying *Drosophila*. We quantified the kinematics of both the initial turn, hereon referred to as the putative "anemometric" turn, and the wind orienting turn, referred to as the "anemotactic" turn. Comparing the

turns along two parameters: turn duration and peak angular velocity, both as a function of turn magnitude, revealed that both turns have kinematic profiles closely matching those of body saccades for either either tethered or free-flying *Drosophila* (Figure 6E,F).

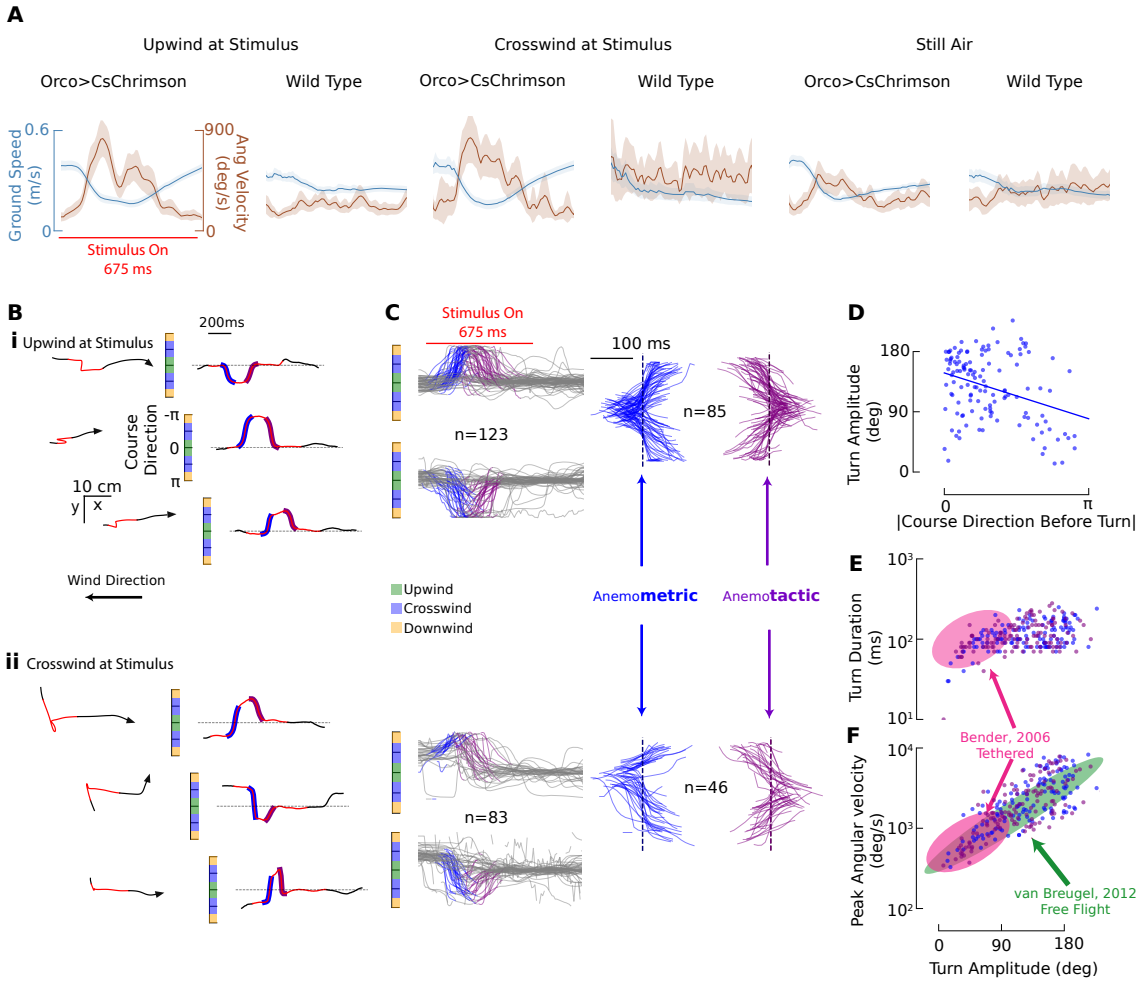

Figure 6. Anemotaxis is often a ballistic two-turn sequence. **A)** Population ground speed and angular velocity profiles for flies which received a flash of red light when entering the trigger zone. Groups were split into flies which were upwind at the time of the stimulus, crosswind at the stimulus, or in still air. **B)** 1.1 second portions of trajectories as they orient into the wind and their associated course direction as a function of time for flies oriented either (i) upwind at the time of stimulus or (ii) crosswind at the stimulus. Course direction plots are highlighted blue for the initial ("anemometric") turn and purple for the wind orienting ("anemotactic") turn. **C)** Course direction vs. time of flies as they orient into the wind, with the two turns extracted and centered around their midpoint to the right. Each anemometric turn has a corresponding anemotactic turn in this analysis. For the crosswind subset the sign of the course direction for some trajectories was modified to better visually display turn regions. **D)** Amplitude of the anemometric turn as a function of the trajectories course at the time of the stimulus. **E)** Turn duration of the anemometric and anemotactic turns as a function of the turn amplitude. Blue markers are for the anemometric turns and purple markers indicate the anemotactic turns. Pink shaded region shows the approximate envelope of saccade kinematics for magnetically tethered *Drosophila* from Fig. 3B in [Bender and Dickinson, 2006b]. **F)** Peak angular velocity of turns as a function turn amplitude for the anemotactic and anemometric turns presented in this study. Pink shading shows the approximate envelope from Fig. 3C in [Bender and Dickinson, 2006b]. Green shading shows the approximate envelope for body saccades made by freely flying *Drosophila* originally reported in Fig. 3H in [Van Breugel and Dickinson, 2012].

DISCUSSION

Summary

Here we establish that, like in larval and walking flies [Kadakia et al., 2022, Matheson et al., 2022, Tao et al., 2023, Odell et al., 2022, Clark et al., 2018, Demir et al., 2020], optogenetic stimulation of *Orco+* neurons induces naturalistic olfactory navigation behaviors in free-flight. We then investigated how flies use information from their wind environment to deploy a plume tracking strategy. In still air flies use a previously uncharacterized plume tracking behavior dominated primarily by two stereotyped motifs: rapid saccades biased in a consistent direction while descending in altitude. In the same way that the casting element of "cast and surge" is a fly's attempt to reconnect with a plume, we demonstrate that the circling element of "sink and circle" is a fly's attempt to reconnect with an odor plume. We hypothesize that sink and circle is likely proximal search strategy to stay nearby to the point of odor loss. Detecting an odor packet in the presence of wind may not necessarily be indicative of proximity to an odor source as an odor packet can travel over large distances when carried by wind. However, detecting an odor in still air may indicate a high likelihood that a fly is close to the source and it is better to search locally.

Implications of circling and candidate supporting circuits

Evidence of circling behaviors can be found in prior modelling and behavioral studies. For example, trajectories of agents using an infotactic search strategy in still air superficially resemble circling flies [Vergassola et al., 2007]. Flying flies searching for an invisible odor in a cylindrical arena also resemble the searching behavior we describe here [Frye et al., 2003, Saxena et al., 2018] and walking flies search with high angular velocities after optogenetic activation of OSNs [Álvarez-Salvado et al., 2018, Corfas et al., 2019]. However, with a real odor, flies can dynamically interact with an odor plume and alternate between bouts of high turn rates while circling interspersed with stretches of straight flight after encountering an odor packet. This has the potential to generate the long-tailed Levy distributions which have been previously associated with scale-free search in free-flying *Drosophila* [Reynolds and Frye, 2007]. Paradigms which can open the behavioral loop for plume tracking are therefore critical for understanding how models of complex search ethology can arise from the building blocks of simpler stereotyped motor programs.

Where in the brain are the motor control commands generated that result in the circling behavior? In the silk moth *Bombyx mori*, crosswind counter turning is likely generated by pairs 'flip flop' neurons in the lateral accessory lobe [Kanzaki and Mishima, 1996]. Saccade directionality and timing in flying flies may be controlled by analogous pairs of neurons [Ros et al., 2023]. Compared to walking moths however, crosswind casting in flies is not simply an alternation of contralateral turns (Figure 3D). The stereotyped, rhythmic and unidirectional turns we describe here may prove to be an ideal candidate for investigating the neural mechanisms underlying long sequences of sensorimotor control.

Reducing altitude may facilitate sampling odor in the boundary layer

We found in both the case of laminar wind and still air flies modulated their altitudes within the wind tunnel in response to a fictive odor experience. One possible explanation is that reducing their flight altitude after encountering an odor may be a strategy convergent with mammalian behavior. Odor packets at higher altitudes and further away from a boundary layer tend to be more dispersed and travel further, whereas close to the boundary layer, odor packets do not travel as far. Canids and murids alternate between episodes of rearing their snouts to sample the air above and then lowering their snout to sniff near the ground inside the boundary layer [Jinn et al., 2020, Gire et al., 2016]. Agent-based modelling approaches suggest that alternating between sniffing out an odor between a high and low vertical position can provide an agent with information necessary to navigate to the source of a complex, three dimensional plume dispersed in turbulent flow-fields [Rigolli et al., 2022]. Like in vertebrates, flies upon encountering an odor packet at a high altitude may gain information by subsequently lowering their altitudes to sample the air beneath themselves.

Anemotactic saccades imply flies possess an internal estimate of wind direction

Our observation that flies orient into the wind using a turn with saccade-like kinematics has important implications for understanding wind guided navigation. Saccades are ballistic, feed-forward motor commands [Bender and Dickinson, 2006a] during which feedback from motion vision is actively suppressed [Kim et al., 2015, Fenk et al., 2021]. This suggests that flies must have an internal estimate of the ambient wind direction in order to generate the feed-forward motor commands that drive their anemotactic turns. The ballistic upwind turns, and the wind-gated decision to circle or surge, indicate that flies have an internal model for both the presence and direction of ambient wind. How flies calculate such an estimate and for how long it persists remains unclear. The behavioral time course in both laminar wind and still air is remarkably similar for the first $\sim$150 ms after odor onset, during which time flies decelerate. We

suggest that this deceleration event and, in the presence of wind, a rapid course change are active sensing maneuvers used to estimate properties of ambient wind.

Putative computational mechanisms for active sensing of wind presence and direction

For a fly flying on a straight course, it would be impossible to uniquely determine if it is moving directly upwind, or flying in still air. Recent control theoretic analyses have shown that if a fly were to decelerate or change course, however, the ways in which the magnitudes and angles of visual motion and apparent wind will change relative to one another can resolve key properties of ambient wind [van Breugel, 2021, van Breugel et al., 2022, Cellini et al., 2023]. Broadly, changes in ground speed may facilitate estimates of wind speed. However, such estimates would require that flies have a calibrated measure of the magnitude of optic flow (see Supplement). This presents a complication because the responses of wide field optic flow sensitive neurons depend on texture and are subject to motion adaptation [Harris et al., 1999].

To address the challenges raised by unknown sensor calibration coefficients, we describe two candidate delay-and-compare mechanisms that could provide flies with a simple binary heuristic for assessing the presence of wind either via a deceleration maneuver or change in course (Figure 7). Both heuristics are robust to unknown sensor calibration coefficients (see Supplement). To assess the presence of wind while decelerating, flies could compare the relative changes in magnitude of airflow (i.e. apparent wind) and optic flow. If there is no wind, then the following must be true: $\log(a_t) - \log(r_t) = \log(a_{t+\Delta t}) - \log(r_{t+\Delta t})$, where a is the magnitude of airflow and r is the magnitude of optic flow (Figure 7A, see Supplement for derivation). An alternative to deceleration would be for the fly to make a change in course. In this case, if there is no wind, then both before and after the turn the angle of optic flow and airflow will be identical (Figure 7B). To make this heuristic robust to unknown sensor calibration coefficients, the fly could compare the relative angles. If there is no wind, then the difference between the optic flow and airflow angles must remain the same after the turn. If there is wind, then the degree to which the angles of optic flow and airflow change across a turning maneuver, in addition to knowledge of the turn's magnitude, can be used to uniquely determine the direction of the ambient wind [van Breugel et al., 2022]. Other angular measurements such as the direction of acceleration could also play a role [van Breugel, 2021]. Based on this theoretical foundation, we refer to the turn flies make prior to turning upwind as a putative "anemometric" saccade.

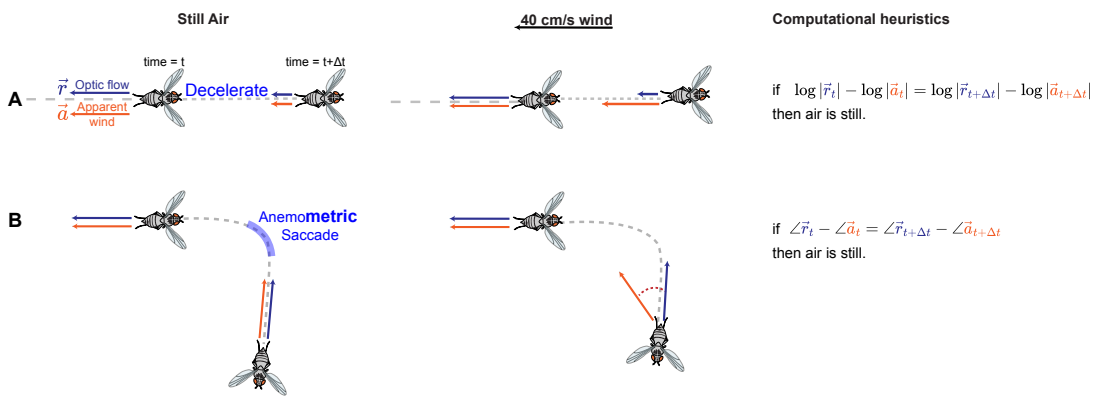

Figure 7. Heuristic models of wind magnitude estimation without cross-calibrated sensory modalities. **A)**. In still air, if a fly decelerates, the relative differences between optic flow and apparent wind magnitude remain constant. **B)** If in still air a fly makes a saccade, then the allocentric angle between its percieved optic flow and airflow will remain constant. Note that the magnitude of the optic flow vector ($\vec{r}$) is both a function of ground speed and altitude, thus its instantaneous magnitude compared to the airspeed magnitude does not provide unique information about the presence of wind; only the relative changes during deceleration would uniquely reveal the presence of wind.

In both still air and in laminar wind flies decelerate to a similar degree, whereas flies are more likely to perform a change in course when there is wind. Thus, we suggest that although flies may use a change in course to simultaneously assess wind presence and direction, we cannot rule out the hypothesis that they use a deceleration maneuver to assess the presence of wind independent of their decision to change course. Whether flies determine the presence and direction of ambient wind according to the candidate mechanisms we describe remains an open question. There is clear evidence that three directional sensory modalities that would enable wind direction estimation are encoded in flies' central complex–the direction of optic flow [Weir et al., 2014, Green et al., 2017], heading relative to landmarks [Seelig and Jayaraman,

2015] or the sky polarization angle [Giraldo et al., 2018], and the direction of apparent wind [Okubo et al., 2020]. The central complex also supports the necessary architecture for angular integration [Green et al., 2017], memory [Grover et al., 2022], vector computations [**?**Lu et al., 2022, Ishida et al., 2023] and turning-synchronized computations [Fisher et al., 2022] that information-gathering during course changes would require. Finally, downstream neurons in the fan-shaped body have been shown to integrate sensory information from key modalities such as vision and airflow [Matheson et al., 2022], making this a likely candidate brain region for computing ambient wind properties.

Circling and flow estimation across taxa

Understanding goal oriented navigation is a central objective of behavioral neuroscience. How organisms modulate their search based on their surrounding flow has critical implications for the likelihood of a successful search event especially for organisms that search over long distances. It would make sense for other organisms to also employ a similar flow-gated strategy as flies. For instance, behavior that is remarkably similar to our observations in flies have been described in Bonnethead sharks in the absence of flow; under these conditions the fish swim in tight circles in the presence of odors and absence of visual cues, which the authors describe as ”area restricted search” (ARS) [Johnsen and Teeter, 1985]. Albatrosses also alternate between bouts of circular search and wind guided navigation while foraging, but circling in this system is attributed to visual features rather than the wind [Nevitt et al., 2008]. From a comparative perspective it is not well understood what sensory cues and internal states trigger area restricted search over long distance navigation. Flow estimation is also likely a general ability across organisms. Although the underlying behaviors and neural mechanisms remain poorly understood, again fish exhibit similarly convergent behaviors and computations to flies. For example, lampreys will execute circling behaviors when they encounter a river plume before swimming upstream [Sorensen et al., 2003], a behavior that may be analogous to the anemometric turns we describe in flies. Meanwhile, zebra fish rely on temporal changes of apparent flow measurements to deduce flow direction during rheotaxis [Oteiza et al., 2017]. The temporal changes of apparent flow are an important component of the theoretical foundations we describe that flies may use to estimate both presence and direction of ambient wind. More broadly, our hypothesis of how flies may estimate wind presence and direction through active turns adds to a growing literature describing how organisms can use motion of their sensors to estimate features of their environment that are not directly measurable [Fenk et al., 2022, Biswas et al., 2023, Ravi et al., 2020, Biswas et al., 2018].

REFERENCES

Alon, U., Surette, M. G., Barkai, N., and Leibler, S. (1999). Robustness in bacterial chemotaxis. *Nature*, 397(6715):168–171.

Álvarez-Salvado, E., Licata, A. M., Connor, E. G., McHugh, M. K., King, B. M., Stavropoulos, N., Victor, J. D., Crimaldi, J. P., and Nagel, K. I. (2018). Elementary sensory-motor transformations underlying olfactory navigation in walking fruit-flies. *Elife*, 7:e37815.

Baker, K. L., Dickinson, M., Findley, T. M., Gire, D. H., Louis, M., Suver, M. P., Verhagen, J. V., Nagel, K. I., and Smear, M. C. (2018). Algorithms for olfactory search across species. *The Journal of Neuroscience*, 38(44):9383–9389.

Barrows, W. M. (1907). *The Reactions of the Pomace Fly: Drosophila ampelophila Loew, to Odorous Substances*.

Bender, J. A. and Dickinson, M. H. (2006a). A comparison of visual and haltere-mediated feedback in the control of body saccades in drosophila melanogaster. *Journal of Experimental Biology*, 209(23):4597–4606.

Bender, J. A. and Dickinson, M. H. (2006b). Visual stimulation of saccades in magnetically tethered drosophila. *Journal of experimental biology*, 209(16):3170–3182.

Benton, R. (2022). *drosophila* olfaction past, present and future. *Proceedings of the Royal Society B Biological Sciences*, 289(1989).

Bhandawat, V., Maimon, G., Dickinson, M. H., and Wilson, R. I. (2010). Olfactory modulation of flight in drosophila is sensitive, selective and rapid. *Journal of Experimental Biology*, 213(21):3625–3635.

Biswas, D., Arend, L. A., Stamper, S. A., Vágvölgyi, B. P., Fortune, E. S., and Cowan, N. J. (2018). Closed-loop control of active sensing movements regulates sensory slip. *Current Biology*, 28(24):4029–4036.

Biswas, D., Lamperski, A., Yang, Y., Hoffman, K., Guckenheimer, J., Fortune, E. S., and Cowan, N. J. (2023). Mode switching in organisms for solving explore-versus-exploit problems. *Nature Machine Intelligence*, 5(11):1285–1296.

Byk, T., Bar-Yaacov, M., Doza, Y. N., Minke, B., and Selinger, Z. (1993). Regulatory arrestin cycle secures the fidelity and maintenance of the fly photoreceptor cell. *Proceedings of the National Academy of Sciences*, 90(5):1907–1911.

Carton, A. and Montgomery, J. (2003). Evidence of a rheotactic component in the odour search behaviour of freshwater eels. *Journal of fish biology*, 62(3):501–516.

Carvalho, T. and Gonçalves, L. F. (2020). Combing the hairy ball using a vector field without equilibria. *Journal of Dynamical and Control Systems*, 26:233–242.

Cellini, B., Boyacıoğlu, B., and van Breugel, F. (2023). Empirical individual state observability. *arXiv preprint arXiv:2304.14313*.

Censi, A., Straw, A. D., Sayaman, R. W., Murray, R. M., and Dickinson, M. H. (2013). Discriminating external and internal causes for heading changes in freely flying drosophila. *PLoS computational biology*, 9(2):e1002891.

Clark, D. A., Odell, S. R., Armstrong, J. M., Turcotte, M., Kohler, D., Mathis, A., Schmidt, D. R., and Mathew, D. (2018). Behavior responses to chemical and optogenetic stimuli in drosophila larvae. *Frontiers in behavioral neuroscience*, 12:324.

Collett, T. S. and Land, M. (1975). Visual spatial memory in a hoverfly. *Journal of comparative physiology*, 100:59–84.

Connor, E. G., McHugh, M. K., and Crimaldi, J. P. (2018). Quantification of airborne odor plumes using planar laser-induced fluorescence. *Experiments in Fluids*, 59:1–11.

Corfas, R. A., Sharma, T., and Dickinson, M. H. (2019). Diverse food-sensing neurons trigger idiothetic local search in drosophila. *Current Biology*, 29(10):1660–1668.

Crall, J., Chang, J., Oppenheimer, R., and Combes, S. (2017). Foraging in an unsteady world: bumblebee flight performance in field-realistic turbulence. *Interface focus*, 7(1):20160086.

Dekker, T. and Cardé, R. T. (2011). Moment-to-moment flight manoeuvres of the female yellow fever mosquito (aedes aegypti l.) in response to plumes of carbon dioxide and human skin odour. *Journal of Experimental Biology*, 214(20):3480–3494.

Demir, M., Kadakia, N., Anderson, H. D., Clark, D. A., and Emonet, T. (2020). Walking drosophila navigate complex plumes using stochastic decisions biased by the timing of odor encounters. *Elife*, 9:e57524.

Dweck, H. K., Ebrahim, S. A., Kromann, S., Bown, D., Hillbur, Y., Sachse, S., Hansson, B. S., and Stensmyr, M. C. (2013). Olfactory preference for egg laying on citrus substrates in drosophila. *Current Biology*, 23(24):2472–2480.

Ejima, A., Smith, B. P., Lucas, C., Van Naters, W. v. d. G., Miller, C. J., Carlson, J. R., Levine, J. D., and Griffith, L. C. (2007). Generalization of courtship learning in drosophila is mediated by cis-vaccenyl

acetate. *Current biology*, 17(7):599–605.
Fenk, L. M., Avritzer, S. C., Weisman, J. L., Nair, A., Randt, L. D., Mohren, T. L., Siwanowicz, I., and Maimon, G. (2022). Muscles that move the retina augment compound eye vision in drosophila. *Nature*, 612(7938):116–122.
Fenk, L. M., Kim, A. J., and Maimon, G. (2021). Suppression of motion vision during course-changing, but not course-stabilizing, navigational turns. *Current Biology*, 31(20):4608–4619.
Fisher, Y. E., Marquis, M., D'Alessandro, I., and Wilson, R. I. (2022). Dopamine promotes head direction plasticity during orienting movements. *Nature*, 612(7939):316–322.
Frye, M. A., Tarsitano, M., and Dickinson, M. H. (2003). Odor localization requires visual feedback during free flight in drosophila melanogaster. *Journal of Experimental Biology*, 206(5):843–855.
Giraldo, Y. M. et al. (2018). Sun navigation requires compass neurons in drosophila. *Current Biology*, 28(17):2845–2852.e4.
Gire, D. H., Kapoor, V., Arrighi-Allisan, A., Seminara, A., and Murthy, V. N. (2016). Mice develop efficient strategies for foraging and navigation using complex natural stimuli. *Current Biology*, 26(10):1261–1273.
Grasso, F. W. and Basil, J. A. (2002). How lobsters, crayfishes, and crabs locate sources of odor: current perspectives and future directions. *Current opinion in neurobiology*, 12(6):721–727.
Green, J., Adachi, A., Shah, K. K., Hirokawa, J. D., Magani, P. S., and Maimon, G. (2017). A neural circuit architecture for angular integration in drosophila. *Nature*, 546(7656):101–106.
Grover, D., Chen, J.-Y., Xie, J., Li, J., Changeux, J.-P., and Greenspan, R. J. (2022). Differential mechanisms underlie trace and delay conditioning in drosophila. *Nature*, 603(7900):302–308.
Harris, R. A., O'Carroll, D. C., and Laughlin, S. B. (1999). Adaptation and the temporal delay filter of fly motion detectors. *Vision research*, 39(16):2603–2613.
Houle, J. and van Breugel, F. (2023). Near-surface wind variability over spatiotemporal scales relevant to plume tracking insects. *Physics of Fluids*, 35(5).
Ishida, I. G., Sethi, S., Mohren, T. L., Abbott, L., and Maimon, G. (2023). Neuronal calcium spikes enable vector inversion in the drosophila brain. *bioRxiv*.
Jinn, J., Connor, E. G., and Jacobs, L. F. (2020). How ambient environment influences olfactory orientation in search and rescue dogs. *Chemical senses*, 45(8):625–634.
Johnsen, P. B. and Teeter, J. H. (1985). Behavioral responses of bonnethead sharks (sphyrna tiburo) to controlled olfactory stimulation. *Marine & Freshwater Behaviour & Phy*, 11(4):283–291.
Kadakia, N., Demir, M., Michaelis, B. T., DeAngelis, B. D., Reidenbach, M. A., Clark, D. A., and Emonet, T. (2022). Odour motion sensing enhances navigation of complex plumes. *Nature*, pages 1–8.
Kanzaki, R. and Mishima, T. (1996). Pheromone-triggered 'fiipflopping'neural signals correlate with activities of neck motor neurons of a male moth, bombyx mori. *Zoological science*, 13(1):79–87.
Kennedy, J. S. et al. (1940). The visual responses of flying mosquitoes. In *Proceedings of the Zoological Society of London*, volume 109. London.
Kennedy, J. S. and Marsh, D. (1974). Pheromone-regulated anemotaxis in flying moths. *Science*, 184(4140):999–1001.
Kim, A. J., Fitzgerald, J. K., and Maimon, G. (2015). Cellular evidence for efference copy in drosophila visuomotor processing. *Nature neuroscience*, 18(9):1247–1255.
Kiselev, A. and Subramaniam, S. (1994). Activation and regeneration of rhodopsin in the insect visual cycle. *Science*, 266(5189):1369–1373.
Leitch, K. J., Ponce, F. V., Dickson, W. B., van Breugel, F., and Dickinson, M. H. (2021). The long-distance flight behavior of drosophila supports an agent-based model for wind-assisted dispersal in insects. *Proceedings of the National Academy of Sciences*, 118(17):e2013342118.
Lingenfelter, B., Nag, A., and van Breugel, F. (2021). Insect inspired vision-based velocity estimation through spatial pooling of optic flow during linear motion. *Bioinspiration & Biomimetics*, 16(6):066004.
Lu, J., Behbahani, A. H., Hamburg, L., Westeinde, E. A., Dawson, P. M., Lyu, C., Maimon, G., Dickinson, M. H., Druckmann, S., and Wilson, R. I. (2022). Transforming representations of movement from body-to world-centric space. *Nature*, 601(7891):98–104.
Marsh, D., Kennedy, J., and Ludlow, A. (1978). An analysis of anemotactic zigzagging flight in male moths stimulated by pheromone. *Physiological Entomology*, 3(3):221–240.
Matheson, A. M., Lanz, A. J., Medina, A. M., Licata, A. M., Currier, T. A., Syed, M. H., and Nagel, K. I. (2022). A neural circuit for wind-guided olfactory navigation. *Nature Communications*, 13(1):4613.
McClain, C. R., Nunnally, C., Dixon, R., Rouse, G. W., and Benfield, M. (2019). Alligators in the abyss: The first experimental reptilian food fall in the deep ocean. *PloS one*, 14(12):e0225345.
Medici, V. and Fry, S. N. (2012). Embodied linearity of speed control in drosophila melanogaster. *Journal of The Royal Society Interface*, 9(77):3260–3267.
Moore, P. and Crimaldi, J. (2004). Odor landscapes and animal behavior: tracking odor plumes in different

physical worlds. *Journal of marine systems*, 49(1-4):55–64.
Nevitt, G. A., Losekoot, M., and Weimerskirch, H. (2008). Evidence for olfactory search in wandering albatross, diomedea exulans. *Proceedings of the National Academy of Sciences*, 105(12):4576–4581.
Odell, S. R., Clark, D., Zito, N., Jain, R., Gong, H., Warnock, K., Carrion-Lopez, R., Maixner, C., Prieto-Godino, L., and Mathew, D. (2022). Internal state affects local neuron function in an early sensory processing center to shape olfactory behavior in drosophila larvae. *Scientific Reports*, 12(1):15767.
Okubo, T. S., Patella, P., D'Alessandro, I., and Wilson, R. I. (2020). A neural network for wind-guided compass navigation. *Neuron*, 107(5):924–940.e18.
Oteiza, P., Odstrcil, I., Lauder, G., Portugues, R., and Engert, F. (2017). A novel mechanism for mechanosensory-based rheotaxis in larval zebrafish. *Nature*, 547(7664):445–448.
Ravi, S., Siesenop, T., Bertrand, O., Li, L., Doussot, C., Warren, W. H., Combes, S. A., and Egelhaaf, M. (2020). Bumblebees perceive the spatial layout of their environment in relation to their body size and form to minimize inflight collisions. *Proceedings of the National Academy of Sciences*, 117(49):31494–31499.
Reynolds, A. M. and Frye, M. A. (2007). Free-flight odor tracking in drosophila is consistent with an optimal intermittent scale-free search. *PloS one*, 2(4):e354.
Riffell, J. A., Shlizerman, E., Sanders, E., Abrell, L., Medina, B., Hinterwirth, A. J., and Kutz, J. N. (2014). Flower discrimination by pollinators in a dynamic chemical environment. *Science*, 344(6191):1515–1518.
Rigolli, N., Reddy, G., Seminara, A., and Vergassola, M. (2022). Alternation emerges as a multi-modal strategy for turbulent odor navigation. *Elife*, 11.
Ros, I. G., Omoto, J. J., and Dickinson, M. H. (2023). Descending control and regulation of spontaneous flight turns in drosophila. *bioRxiv*.
Saxena, N., Natesan, D., and Sane, S. P. (2018). Odor source localization in complex visual environments by fruit flies. *Journal of Experimental Biology*, 221(2):jeb172023.
Schone, H. (2014). *Spatial orientation: The spatial control of behavior in animals and man*, volume 588. Princeton University Press.
Seabold, S. and Perktold, J. (2010). statsmodels: Econometric and statistical modeling with python. In *9th Python in Science Conference*.
Seelig, J. D. and Jayaraman, V. (2015). Neural dynamics for landmark orientation and angular path integration. *Nature*, 521(7551):186–191.
Sharkey, C. R., Blanco, J., Leibowitz, M. M., Pinto-Benito, D., and Wardill, T. J. (2020). The spectral sensitivity of drosophila photoreceptors. *Scientific Reports*, 10(1).
Singh, S. H., van Breugel, F., Rao, R. P., and Brunton, B. W. (2023). Emergent behaviour and neural dynamics in artificial agents tracking odour plumes. *Nature Machine Intelligence*, 5(1):58–70.
Sorensen, P., Vrieze, L., and Fine, J. (2003). A multi-component migratory pheromone in the sea lamprey. *Fish Physiology and Biochemistry*, 28:253–257.
Straw, A. D., Branson, K., Neumann, T. R., and Dickinson, M. H. (2010a). Multi-camera real-time three-dimensional tracking of multiple flying animals. *Journal of The Royal Society Interface*, 8(56):395–409.
Straw, A. D., Lee, S., and Dickinson, M. H. (2010b). Visual control of altitude in flying drosophila. *Current Biology*, 20(17):1550–1556.
Tao, L., Wechsler, S. P., and Bhandawat, V. (2023). Sensorimotor transformation underlying odor-modulated locomotion in walking drosophila. *Nature Communications*, 14(1):6818.
van Breugel, F. (2021). A nonlinear observability analysis of ambient wind estimation with uncalibrated sensors, inspired by insect neural encoding. In *2021 60th IEEE Conference on Decision and Control (CDC)*, pages 1399–1406. IEEE.
Van Breugel, F. and Dickinson, M. H. (2012). The visual control of landing and obstacle avoidance in the fruit fly drosophila melanogaster. *Journal of Experimental Biology*, 215(11):1783–1798.
van Breugel, F. and Dickinson, M. H. (2014). Plume-tracking behavior of flying drosophila emerges from a set of distinct sensory-motor reflexes. *Current Biology*, 24(3):274–286.
van Breugel, F., Huda, A., and Dickinson, M. H. (2018). Distinct activity-gated pathways mediate attraction and aversion to co2 in drosophila. *Nature*, 564(7736):420–424.
van Breugel, F., Jewell, R., and Houle, J. (2022). Active anemosensing hypothesis: how flying insects could estimate ambient wind direction through sensory integration and active movement. *Journal of The Royal Society Interface*, 19(193).
Van Breugel, F., Liu, Y., Brunton, B. W., and Kutz, J. N. (2022). Pynumdiff: A python package for numerical differentiation of noisy time-series data. *Journal of Open Source Software*, 7(71):4078.
Van Breugel, F., Morgansen, K., and Dickinson, M. H. (2014). Monocular distance estimation from optic flow during active landing maneuvers. *Bioinspiration & biomimetics*, 9(2):025002.

Vergassola, M., Villermaux, E., and Shraiman, B. I. (2007). 'infotaxis' as a strategy for searching without gradients. *Nature*, 445(7126):406–409.

Virtanen, P., Gommers, R., Oliphant, T. E., Haberland, M., Reddy, T., Cournapeau, D., Burovski, E., Peterson, P., Weckesser, W., Bright, J., van der Walt, S. J., Brett, M., Wilson, J., Millman, K. J., Mayorov, N., Nelson, A. R. J., Jones, E., Kern, R., Larson, E., Carey, C. J., Polat, İ., Feng, Y., Moore, E. W., VanderPlas, J., Laxalde, D., Perktold, J., Cimrman, R., Henriksen, I., Quintero, E. A., Harris, C. R., Archibald, A. M., Ribeiro, A. H., Pedregosa, F., van Mulbregt, P., and SciPy 1.0 Contributors (2020). SciPy 1.0: Fundamental Algorithms for Scientific Computing in Python. *Nature Methods*, 17:261–272.

Weir, P. T., Schnell, B., and Dickinson, M. H. (2014). Central complex neurons exhibit behaviorally gated responses to visual motion in drosophila. *Journal of Neurophysiology*, 111(1):62–71.

MATERIALS AND METHODS

Animal Handling

All *Drosophila melanogaster* were maintained in a temperature (25°C) and humidity controlled incubator (60% RH) on a 16:8 light:dark cycle. All flies were reared on standard fly media (Nutrifly, Genesee Scientific, San Diego, CA, USA). The F1 flies from crosses for experiments involving optogenetic stimulation were reared in a fresh media bottle pre-treated with 400 μL of a 40 mM ATR solution (ATR, R2500, Sigma Aldrich)and maintained on the fresh ATR enriched media for at least 48 hours prior to experimentation. Experimental flies (2-5 days old) were anesthetized at 4 °C on a cold plate, and 15 females were placed in an empty tube with a moist Kimwipe to prevent desiccation. We then starved flies in their preparation tubes for 6-8 hours in the morning prior to any experimentation to encourage flight and food seeking. In the evening, we placed experimental flies into the wind tunnel behavioral system without any further anesthesia. Flies were permitted to fly about the tunnel volume overnight until the following morning at which point the data collection was terminated. All experiments included a minimum of three nights of replication.

Behavioral Arena

Wind tunnel

Our free flight behavioral arena consisted of a custom-built wind tunnel with a 1.0x0.5x0.5 m^3 working section (Figure 1A), housed in a room maintained at 22° C and 60% RH. While experiments were running, we continuously ran a carbon air filtration system (SS-422, Sentry Air Systems, Cypress, TX, USA) to remove ambient odors. The airflow in the wind tunnel was generated by an array of computer fans controlled by an Arduino Mega 2560 board. For laminar wind experiments, we set the wind speed in the tunnel to 40 cm/s (calibrated using an ultrasonic anemometer: Trisonica Mini, Anemoment LLC / LiCor, Longmont, CO, USA). For still air experiments, all conditions were the same with the exception that the wind tunnel fans were not running, and we confirmed that there was no appreciable air flow within the wind tunnel using an anemometer.

For illumination within the tunnel, we outfitted each wall of the wind tunnel with arrays of blue LEDs (STN-BBLU-B6A-08C1M-24V, Super Bright LEDs Inc. St. Louis, MO, USA) and infrared LEDs (PN: 7031, Waveform Lighting, Vancouver, WA, USA). The side walls and bottom were lined with a light diffusing film (Spye Smoke, Spyeglass, Minneapolis, MN) to generate smooth infrared lighting over the wall surface (Figure 1A). Infrared LED's lined the entirety of each wall to generate an imperceptible bright background to track flies against. The blue LED's homogenously illuminated the wind tunnel floor, but were arranged along the wind tunnel walls to create an ombré effect that tapered from blue on the wind tunnel floor to black towards the wind tunnel roof. Along the wind tunnel floor we placed a grid of dark, infrared transmissible film, to create a checkerboard effect and provide flies with visual contrast. For experiments investigating attraction to a visual feature on the wind tunnel floor, we did not include the checkerboard lattice and instead placed one dark, infrared transmissible acrylic disk (3.8 cm diameter) on the wind tunnel floor. We complemented the blue and infrared illumination in the wind tunnel with an array of white LEDs that ran along either side of the top of the wind tunnel to provide sufficient orange wavelength light for photoreceptor reisomerization [Byk et al., 1993, Kiselev and Subramaniam, 1994]. Total illumination of the combined white and blue lighting in the wind tunnel was 425 lux in the wind tunnel center, measured by a LX1330B light sensor (Dr. Meter, Hong Kong).

3-D Tracking

Real time 3-D tracking of flies was performed at 100 hz using an array of 12 Basler cameras (acA720, Basler AG, Ahrensburg, Germany) positioned above the wind tunnel (Figure 1A). Cameras were equipped with IR-pass filters so that tracking was performed using only infrared light. 3-D tracking was implemented

in the open source Braid software [Straw et al., 2010a]. All cameras' intrinsic warping parameters were calibrated using a back illuminated 5x7 inch checkerboard and the built-in checkerboard calibration functionality within Braid.

Optogenetic Stimulus and Experimental Paradigm

Experimental paradigms were developed using custom software in C++ and Python, and coordinated with the tracking software via the Robot Operating System (ROS). Our optogenetic stimulus paradigm used the real time 3-D position of a fly to inform a triggering function which was activated when the fly crossed into a pre-defined "trigger zone" within the wind tunnel (Figure 1B). When a fly entered the trigger zone it was randomly assigned either a pulse of light, referred to as "flash" throughout, or no light pulse, referred to as "sham". The optogenetic stimulus itself was generated by powering the red channel of two arrays of Triple Bright RGB LEDs (SparkFun Electronics, Niwot, CO, USA) that lined both the left and right-hand sides of the top of the wind tunnel (Figure 1A). Because the light environment was not entirely homogeneous we generated a 3-D model of the intensity of red light within the trigger zone of the wind tunnel, the average of which is our reported stimulus intensity, 42 μ W mm^{-2} (Supplemental Figure 2). The delay between tracking software and activation of the optogenetic stimulus array was approximately 6 ms. Because 6 ms was less than the interval between individual camera frames, we considered the optogenetic stimulus delay to be negligible for the purposes of our analyses. We included random sham triggering events to account for the closed loop behavior of what a fly would naturally do in the wind tunnel volume in the absence of any kind of optogenetic perturbation. The sham trajectories provided a secondary control to estimate whether or not there were any visually mediated artifacts from flashing the array of red LEDs. For flies that triggered a light flash, the stimulus consisted of a 675 ms continuous pulse of light unless otherwise noted. Experiments included a 5 second refractory period during which flies could not reactivate a triggering event. Because trajectories could enter a far upwind or downwind zone within the wind tunnel where tracking was not possible, we were often limited to only a few seconds of behavior after each triggering event. We therefore restrict most analyses to the 3 second period directly after a flash or sham event.

Plume Generation

For the subset of experiments which involved an ethanol plume, we continuously pumped air through a 50% ethanol solution and up through a port that arose from the bottom of the wind tunnel on the far upwind end. We controlled the flow rate of the plume at 130 cm^3 /minute using a digital mass flow control system (Alicat Scientific, Tuscon, AZ, USA). The port was connected to a 25 cm tall rigid acrylic tube that was bent at a 90°angle and with its open face covered in a metallic mesh to prevent flies from entering the tubing. This generated an ethanol plume in approximately the same volume as the optogenetic trigger zone.

Trajectory Inclusion Criteria and Data Filtering

For all optogenetic experiments, we included only trajectories which specifically elicited a triggering event (flash or sham). We also only included trajectories for which we had at least one full second of tracking after the triggering event before losing track of the fly when it entered an occluded zone within the wind tunnel. In the unlikely occasion that the same trajectory re-triggered the optogenetic stimulus we restricted analyses only to the first triggering instance for a given trajectory. On rare occasions, we found trajectories with brief jagged portions. We filtered these trajectories by excluding data points where a fly's ground speed was greater than 2.0 m/s, an uncharacteristically high ground speed for *Drosophila melanogaster* flying either outdoors, or in a constrained space [Leitch et al., 2021, Straw et al., 2010b, Medici and Fry, 2012]. Additionally, because angular velocity measurements twice propagate the derivatives of tracking noise from flies' x and y position, we found that angular velocity estimates on occasion experience brief highly variable segments along a trajectory. To account for this in our angular velocity analyses, we implemented a Butterworth Filter on the trajectory course direction before first order finite differentiation, all implemented in Python using the PyNumDiff package [Van Breugel et al., 2022].

Saccade Detection

Fly fruit flies typically change course via rapid turns referred to as body saccades [Collett and Land, 1975]. To identify and characterize saccades, we used a slightly modified version of the Geometric Saccade Detection algorithm found in [Censi et al., 2013]. Our primary modification to the original algorithm was to include a term that took a trajectory's ground speed into account in determining where saccades occurred, details are provided in the Supplemental Materials. We visually inspected trajectories for agreement on saccade annotations (Supplemental Figure 1). We did find that some trajectories included erroneous saccade labelling, likely arising from tracking noise that resulted from a fly leaving the field of view of one tracking camera or entering the field of view of another. We excluded these trajectories (¡15% of all trajectories) from analyses but the decision to include or remove them had no noteworthy impacts

on conclusions drawn from the data. Kinematic properties of saccades were determined by isolating the portion of the trajectory 70 ms before and 70 ms after the saccade annotation.

A Note on Experimental Flies, Genetic Controls, and Characterizing Visually Mediated Artifacts

Motivated by prior optogenetic activation experiments with walking flies [Kadakia et al., 2022, Bhandawat et al., 2010, Álvarez-Salvado et al., 2018, Corfas et al., 2019], we chose to express the red-light sensitive ion channel, CsChrimson in olfactory receptor neurons that express the co-receptor *Orco* using the UAS/Gal4 binary expression system. Although *Orco+* neurons mediate a broad range of olfactory responses that are linked to odors with a range of valences [Dweck et al., 2013, Ejima et al., 2007], the behaviors we observed by activating *Orco+* neurons (detailed in results) are remarkably consistent with published free flight responses of *Drosophila* tracking ethanol and vinegar plumes in flight (Figure 1) [van Breugel and Dickinson, 2014].

Unlike much of the prior work in walking flies, however, we could not use visually blinded flies because flight requires visual feedback. This raises the possibility of inducing visually mediated startle responses from sudden flashes of red light, despite flies' relatively low red light sensitivity [Sharkey et al., 2020]. This is further complicated by standard genetic practices which use flies made in genetic backgrounds with a loss of function mutation in the *White* gene, the protein product of which is necessary for synthesizing the red screening pigments in the adult fly eyes. We therefore elected to use experimental flies which were at least heterozygous for a wild-type copy of *White* (Table 1). To characterize any visually mediated startle responses from red light flashes in genetic controls, we prioritized matching the *White* genotype of our Orco>CsChrimson flies (Supplemental Figure 3). Our paradigm resulted in negligible visually mediated artifacts in two genetic controls: CsChrimson/+ flies and wild-type flies. We did find that our Orco>CsChrimson flies raised on media which had no ATR supplementation were moderately responsive to red light flashes. However, we attributed this as more likely due to weak OSN activation rather than a visual response because they displayed a weak, time delayed anemotaxis behavior (Supplemental Figure 3). After establishing that there were no salient visually mediated startle effects and due to the time consuming nature of our behavioral experiments, we elected to simply use wild-type flies as genetic controls for experiments in still air.

Statistical Analyses

All statistical analyses were performed in Python 3.8 using SciPy Stats version 1.9.2 [Virtanen et al., 2020] or StatsModels [Seabold and Perktold, 2010]. Because we could not maintain fly identity over the course of an experiment, we assumed all trajectories are independent samples. Each experiment presented however, is the compilation of a minimum of 3, 16 hour recording periods from at least 45 independent flies. For all saccade specific analyses we considered saccades to be independent events, although we verified that if we instead averaged the properties of saccades from each individual trajectory and use each trajectory as an independent sample, the results are consistent. Data are reported in terms of means and standard deviations. Error shading on graphical representations of data represent 95% confidence intervals.

AUTHOR CONTRIBUTIONS

Study conception and design: SDS and FvB. Data collection: SDS. Analysis and interpretation of results: SDS and FvB. Manuscript preparation: SDS and FvB.

DATA AVAILABILITY

All data and code used to generate analyses will be made publicly available upon publication.

FUNDING

This work is supported by: NIH (P20GM103650); AFOSR (FA9550-21-0122); Sloan (FG-2020-13422), all to FvB.

ACKNOWLEDGEMENTS

We would like to thank Dr. Kathy Nagel for sharing *Drosophila* lines and for providing critical feedback at several stages of this project. We would also like to thank Dr. Dennis Mathew and Dr. Tom Kidd who provided invaluable assistance and feedback from the early stages of this work. We would like to acknowledge Austin Lopez for assistance with the wind tunnel and Kaylee Jamison for assistance with fly care and preparation. We would like to thank all of the members of the van Breugel lab who contributed ideas and suggestions for this manuscript from its nascent stages.

REAGENTS

Experimental Animals		
Experimental Genotype	Parental Strain (s)	Source
NorpA/+;Orco-Gal4/+;UAS-CsChrimson/+	NorpA;Orco-Gal4;UAS-CsChrimson and Heisenberg-CantonS	Dr. Katherine Nagel Dr. Michael Dickinson
Wild Type	Heisenberg-CantonS	Dr. Michael Dickinson
UAS-CsChrimson/+	UAS-CsChrimson and Heisenberg-CantonS	BDSC_55135 Dr. Michael Dickinson

SUPPLEMENTARY MATERIAL

S1. Modified Geometric Saccade Detection Algorithm (mGSD)

For saccade analyses and annotation of where saccade events occurred, we adapted a modified version of the Geometric Saccade Detection Algorithm found in [Censi et al., 2013] Supplemental section 7.1. We calculated the mGSD score as follows.

1) For a given flight trajectory in the horizontal plane define a trajectory as $p\langle k\rangle = \langle x(k), y(k)\rangle$ where x and y are the x and y positions of the fly at frame k. Here k is an integer ranging from 1 (the first frame in the region of interest of a given trajectory) to n (the last frame in the region of interest along a trajectory).

2) Define a time step δ, in our case 5 frames (50ms), and for all k from 1+δ to n-δ). Redefine the origin of the coordinate frame so that $\langle x(\bar{k}), y(\bar{k})\rangle = \langle 0, 0\rangle$.

3) For each $\bar{k}$ define two intervals, the "before" interval $[\bar{k}-\delta, \bar{k}-1]$ and an "after" interval $[\bar{k}+1, \bar{k}+\delta]$.

4) For both the before and after intervals, calculate the angle, θ of each $\langle x(k), y(k)\rangle$ with respect to the new origin.

5) We define two angles, θ_{before} and θ_{after}, as the median angle of the before and after intervals respectively. We then define an amplitude score at $\bar{k}$, $A(\bar{k})$, as:

$$A(\bar{k}) = |\theta_{after} - \theta_{before}|.$$

6) We then calculate a dispersion score, $D(\bar{k})$ based on the horizontal distance travelled by a fly within +/- δ around $\bar{k}$. We define the dispersion parameter as the standard deviation of the flies linear distance from the newly defined origin over the $[\bar{k}-\delta, \bar{k}+\delta]$ interval.

7) At $\bar{k}$ the mGSD score, $S(\bar{k})$, is then:

$$S(\bar{k}) = A(\bar{k})D(\bar{k}).$$

8) To determine at which frames a saccade event occurred we selected a threshold score for $S(\bar{k})$ of 0.001. We then found all continuous regions over a trajectory where the saccade score was greater than our threshold, and during which it did not drop below the threshold for more than 5 frames in a row. We then annotated saccade events as the median position of the trajectory of each of these continuous runs where the score was over the threshold.

S2. Volumetric Stimulus Calibration

We generated a 3-D model of the light intensity within the trigger zone volume by coupling the real time Braid tracking with light intensity measurements from an FDS100 photodiode (Thor Labs, Ann Arbor, MI, USA). We constructed a module that housed four infrared LED's equidistant from the photodiode (Figure S2A). We inferred the photodiode position as the centroid of the four infrared LED positions, which were tracked using Braid (Figure S2B). We slowly moved the light measurement module throughout the volume of the wind tunnel with all of the room and wind tunnel lights turned off except for both of the arrays of red LED's which lined the top of the wind tunnel. While moving the light measurement module we synchronously recorded the photodiode position and a voltage measurement from the photodiode itself (Figure S2C). We converted raw voltage measurements to light intensity measurements using the FDS100 data sheet and assuming a red light wavelength of 630 nm. From the raw position measurements we created a 3-D mesh of the light intensity within the volume of the pre-defined trigger zone (Figure S2D). Our reported stimulus is the mean light intensity in the trigger zone mesh, 42 μ W mm^{-2}.

S3. Derivation a heuristic visual anemometry model for assessing the presence of wind during deceleration

To determine wind speed, a fly would need to integrate information about its perceived airflow[1] with an estimate of its ground velocity. Although insects cannot directly measure ground velocity, they do have access to the magnitude of ventral optic flow, which provides information about the ratio of ground velocity to their altitude above the ground (ventral optic flow can be written as $\vec{r} = -\vec{g}/d$, where $\vec{r}$ is the optic flow vector, $\vec{g}$ is the ground velocity, and d is the altitude). A simple solution would be for a fly to decelerate

[1] Note: flies could determine the airflow magnitude using their antennae. Alternatively, flies could measure the forces on their wings using strain sensors, or use the level of power muscle activity together with an internal model of how that level of activity translates to wing forces.

until it is hovering relative to its visual reference. However, we found that on average flies do not slow down to that extent. By accelerating or decelerating, it would be feasible for an insect to estimate its ground speed and the distance to objects [Van Breugel et al., 2014, Lingenfelter et al., 2021], and by extension, wind speed as well [Cellini et al., 2023]. Such a calculation would, however, require that the magnitude of optic flow is accurate and calibrated. The responses of wide field optic flow sensitive neurons in flies are, however, dependent on spatial frequency and subject to motion adaptation [Harris et al., 1999], making accurate estimates difficult. For these reasons we propose simple heuristics that are independent of sensor calibration constants.

To assess the presence of wind flies could compare the relative changes in magnitude of airflow and optic flow across a deceleration maneuver. To illustrate how this could work, consider a scenario where a fly is maintaining a constant altitude in constant wind, or in still air. We can write down the following expressions for uncalibrated measurements of ventral optic flow ($k \cdot \vec{r}$) and air flow ($q \cdot \vec{a}$), taken from before and after a deceleration maneuver (or at any point during the maneuver):

$$\begin{aligned} k \cdot \vec{r}_t &= \vec{g}_t / d, \\ k \cdot \vec{r}_{t+\Delta t} &= \vec{g}_{t+\Delta t} / d, \end{aligned} \tag{1}$$

$$\begin{aligned} q \cdot \vec{a}_t &= \vec{w} + \vec{g}_t, \\ q \cdot \vec{a}_{t+\Delta t} &= \vec{w} + \vec{g}_{t+\Delta t}, \end{aligned} \tag{2}$$

where d is the fly's altitude, $\vec{g}_{t,t+\Delta t}$ are the unknown ground velocity vectors at two points along the trajectory, $\vec{w}$ is the unknown constant wind velocity vector, q is an unknown calibration constant for airflow measurements, and k is an unknown calibration constant for optic flow measurements (which we also use to absorb the minus sign from the definition of $\vec{r}$). Comparing the measurements across time we can write the following expressions,

$$\begin{aligned} (\vec{a}_{t+\Delta t} - \vec{a}_t)/\vec{a}_t &= (\vec{g}_{t+\Delta t} - \vec{g}_t)/(\vec{w} + \vec{g}_t), \\ (\vec{r}_{t+\Delta t} - \vec{r}_t)/\vec{r}_t &= (\vec{g}_{t+\Delta t} - \vec{g}_t)/\vec{g}_t. \end{aligned} \tag{3}$$

Note that the calibration constants k and q cancel out. Now we can write the following heuristic to assess the presence of wind: if $(\vec{a}_{t+\Delta t} - \vec{a}_t)/\vec{a}_t = (\vec{r}_{t+\Delta t} - \vec{r}_t)/\vec{r}_t$, then there is no wind (i.e. $\vec{w} = 0$). Otherwise, there must be some level of ambient wind. To make it clearer how such a comparison might be implemented in a neural circuit, we can simplify the expression to the following comparison of ratios

$$\vec{a}_{t+\Delta t}/\vec{a}_t = \vec{r}_{t+\Delta t}/\vec{r}_t. \tag{4}$$

We can further simplify by taking only the magnitude portion of the airflow and optic flow vectors as follows

$$|\vec{a}_{t+\Delta t}|/|\vec{a}_t| = |\vec{r}_{t+\Delta t}|/|\vec{r}_t|. \tag{5}$$

The ratio can be converted into simple subtraction, an operation potentially more easily computed by neural circuit architectures, by using a log transform

$$\log(|a_{t+\Delta t}|) - \log(|a_t|) == \log(|r_{t+\Delta t}|) - \log(|r_t|), \tag{6}$$

which we can rearrange to

$$\log(|a_t|) - \log(|r_t|) = \log(|a_{t+\Delta t}|) - \log(|r_{t+\Delta t}|). \tag{7}$$

This final expression shows how the relative magnitudes of airflow and optic flow from before and after a deceleration maneuver can be used to assess the presence of wind.

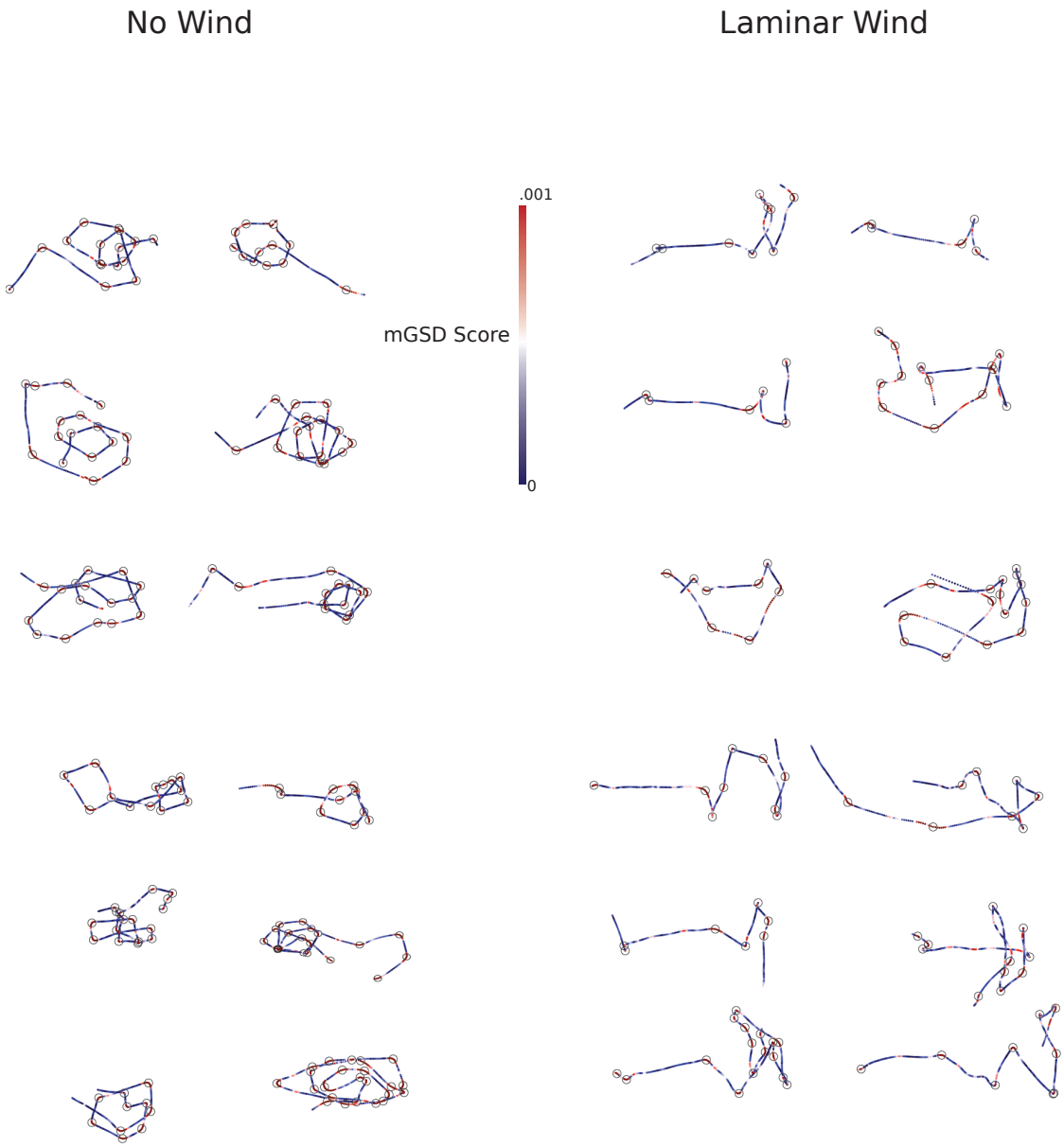

Supplementary Figure S1. Sample trajectories of Orco>CsChrimson flies which received an optogenetic stimulus (12 from still air conditions (Left) and 12 from laminar wind conditions (Right) color coded by the mGSD score at each point. Black circles indicate locations of saccades as determined by the mGSD algorithm.

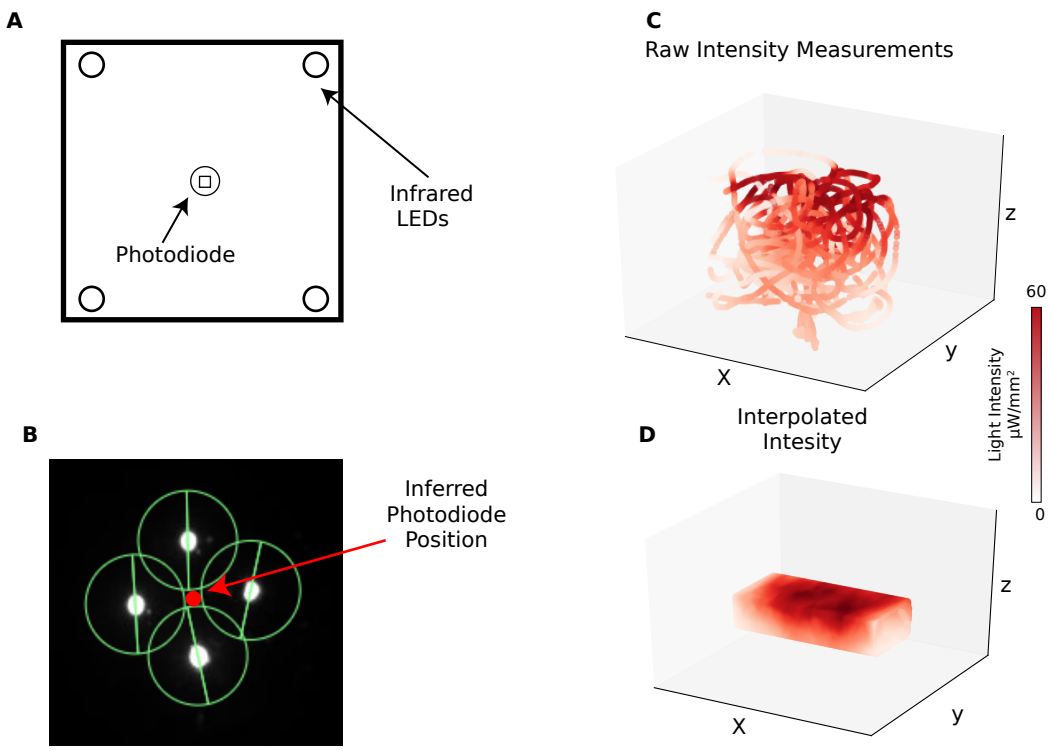

Supplementary Figure S2. Three dimensional calibration of red light intensity in the wind tunnel volume. **A)** Schematic of light measurement module with four infrared LEDs for tracking and a photodiode in the middle. **B)** Example of tracking on four LED's with inferred position of the photodiode position from the infrared LEDs. **C)** Raw position and light intensity measurements from synchronized tracking and photodiode recordings. **D)** Interpolated light intensity in the trigger volume.

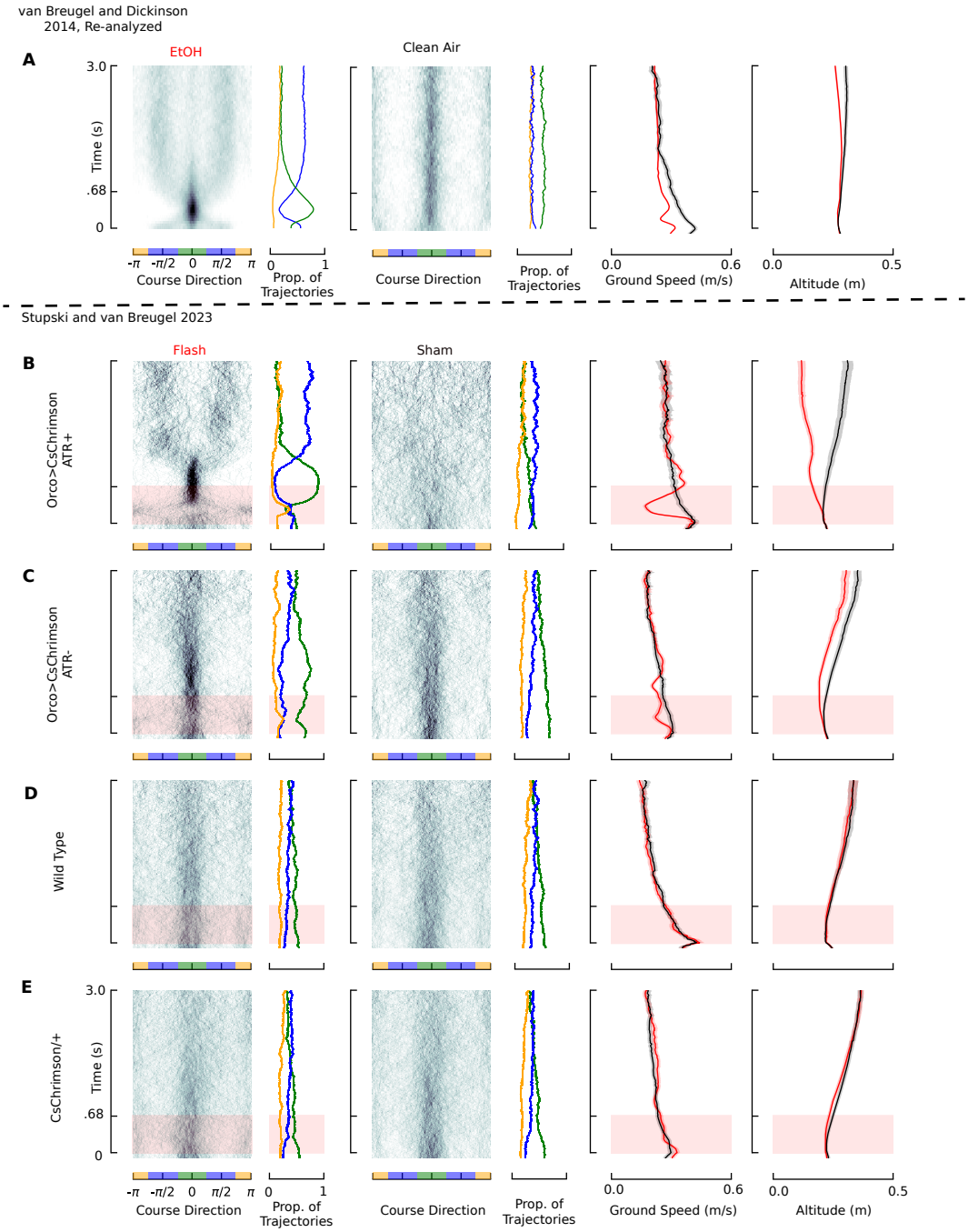

Supplementary Figure S3. Comparison of Orco>CsChrimson optogenetic activation to wild-type flies encountering an ethanol plume, and genetic controls. **A)** Reanalysis of data from [van Breugel and Dickinson, 2014] where wild-type flies encountered a narrow plume of ethanol. Here we analyze the data using the same time scales and graphical parameters as our Orco>CsChrimson experiments shown in Figure 1D and repeated here in panel B. For the flies encountering ethanol, instead of ”flashes” and ”shams”, analyses are generated from the separate ethanol (red trace, n=2487) and clean air (black trace, n=942) experiments. **B)** Orco>CsChrimson data, repeated from Figure 1D to aid direct visual comparison to other data sets (n=232 flash trajectories, n=222 sham trajectories). **C)** ATR- control. Orco>CsChrimson flies in the same behavioral paradigm as panel B, except these flies were reared without ATR enriched media (n=357 flash trajectories, n=350 sham trajectories). **D)** Wild-type Flies. Repeated from Figure 1D to aid direct visual comparison (n=398 flash, n= 429 sham). **E)** UAS-CsChrimson/+ heterozygotes subject to the same paradigm used in panels B-E. Used to establish that there were no salient visually mediated artifacts from red light flashing associated with *White* heterozygosity (n=682 flash trajectories, n=683 sham trajectories)

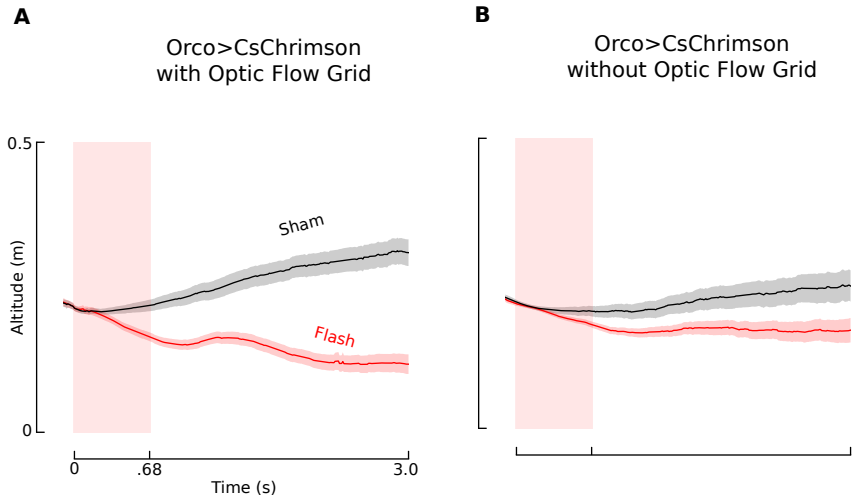

Supplementary Figure S4. Flies' reduce altitude after virtual odor stimulus regardless of the visual contrast on the floor of the wind tunnel. **A)** Altitude dynamics of Orco>CsChrimson flies with a high contrast checkerboard grid on the floor of the wind tunnel (n= 263 flash trajectories; n=291 sham trajectories). **B)** Same as A, but without a checkerboard grid on the floor of the tunnel (n= 740 flash trajectories, n= 786 sham trajectories).

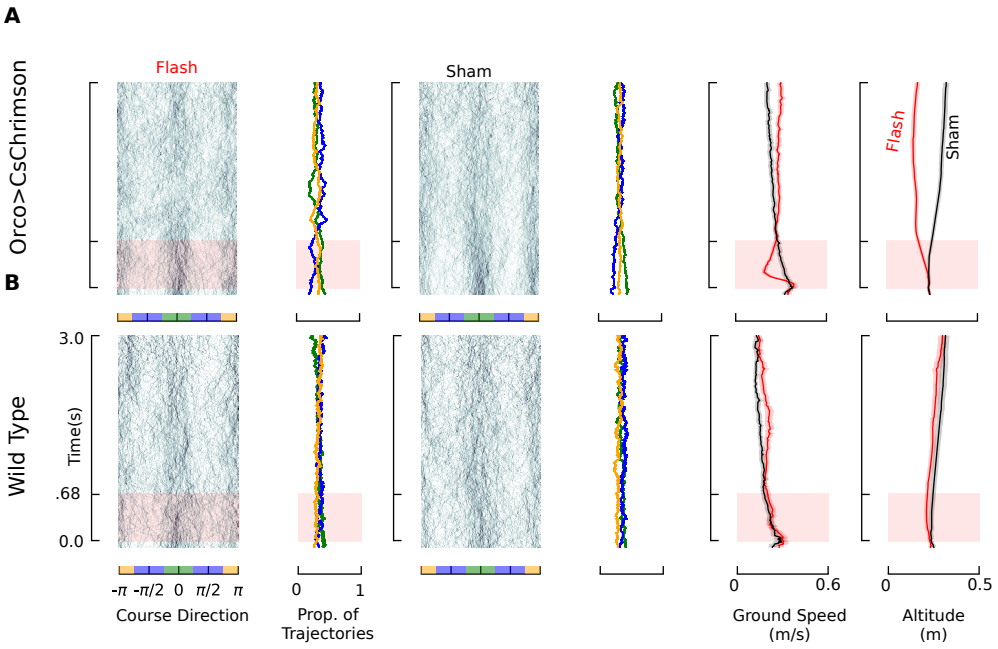

Supplementary Figure S5. Wild-type Control for still condition. **A)** Orco>CsChrimson flies repeated from Figure 1C to aid in direct comparisons (n=263 flash; n=291 sham). **B)** Wild-type control data for no wind flash and sham conditions (n=187 flash trajectories; n=184 sham trajectories).

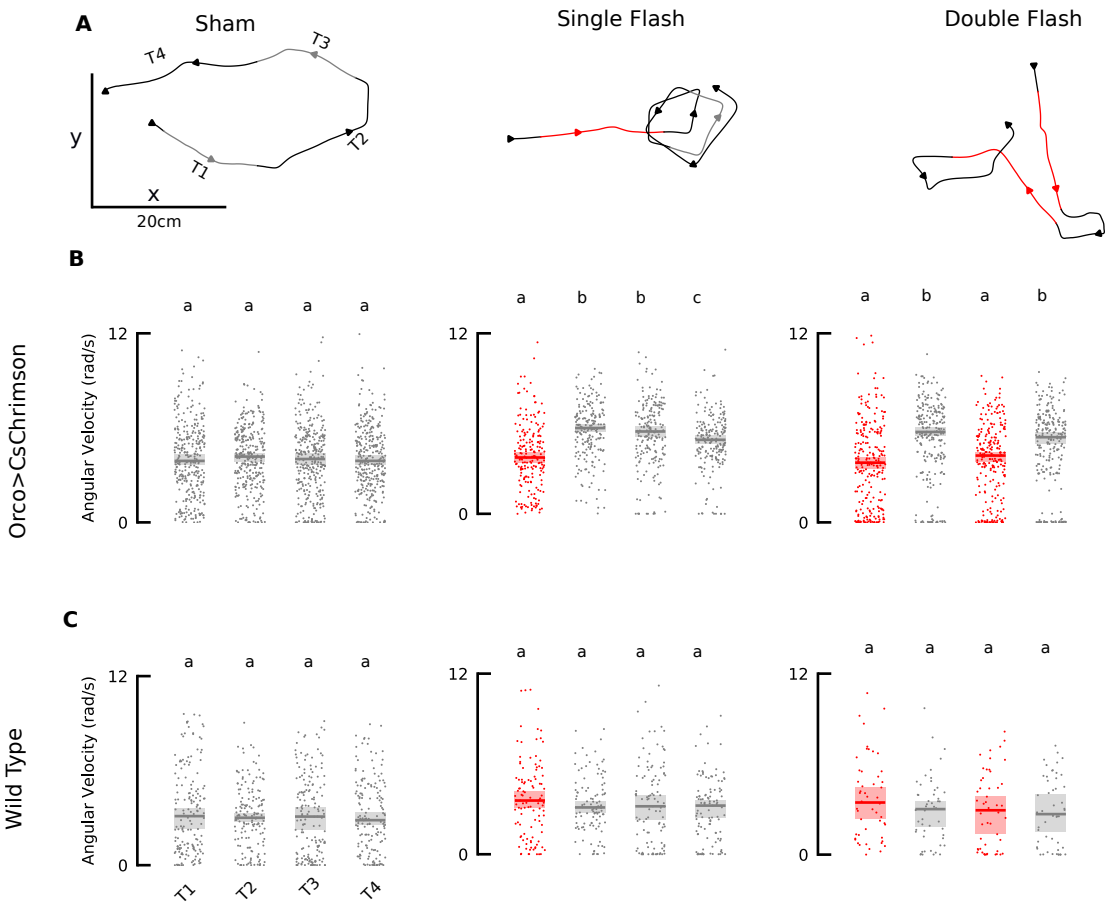

Supplementary Figure S6. Wild-type control for double flash experiments. **A-B)** Repeated from Figure 4 A,C to aid in direct comparison of the data. **C)** Wild-type control for double pulse experiment, analyzed and plotted as in Figure 4C for the sham condition (n=163 trajectories), single flash condition (n=107 trajectories), or the double flash condition (n=50 trajectories). Letters indicate statistical groupings within a genotype and stimulus regimen (Mann-Whitney U test, Bonferroni corrected α = .0083)

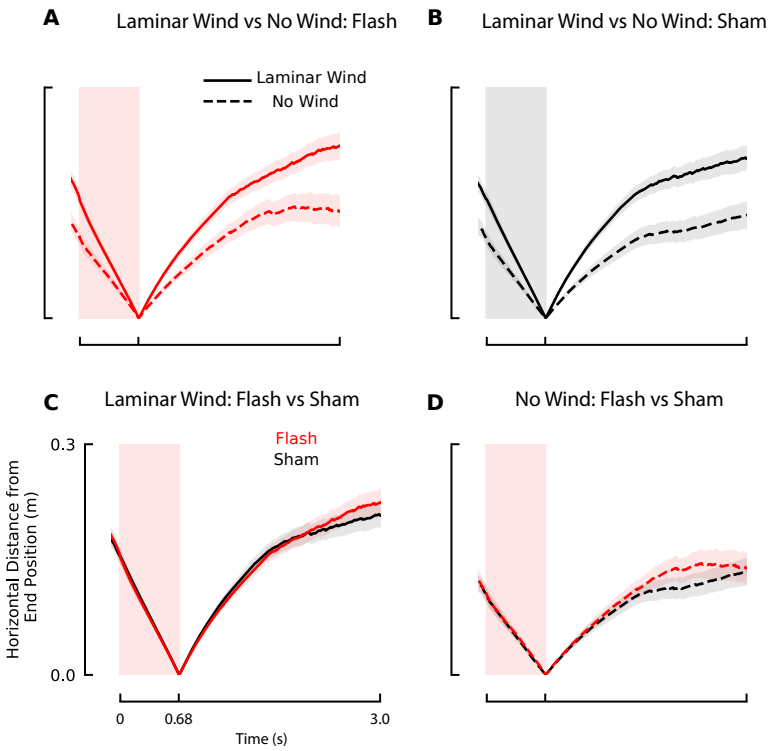

Supplementary Figure S7. Wild-type control for proximal search analysis. **A)** Distance from stimulus end position between wild-type fly trajectories which received a light flash in laminar wind (solid line, n=398 trajectories) or still air (dashed line, n=187 trajectories). **B)** same as **A** but for sham trajectories (laminar wind n= 429 trajectories; still air n= 184 trajectories) **C)** Side by side comparison for wild type trajectories in laminar wind which received either a flash (red) or a sham (black). **D)** Same as **C** for still air case.

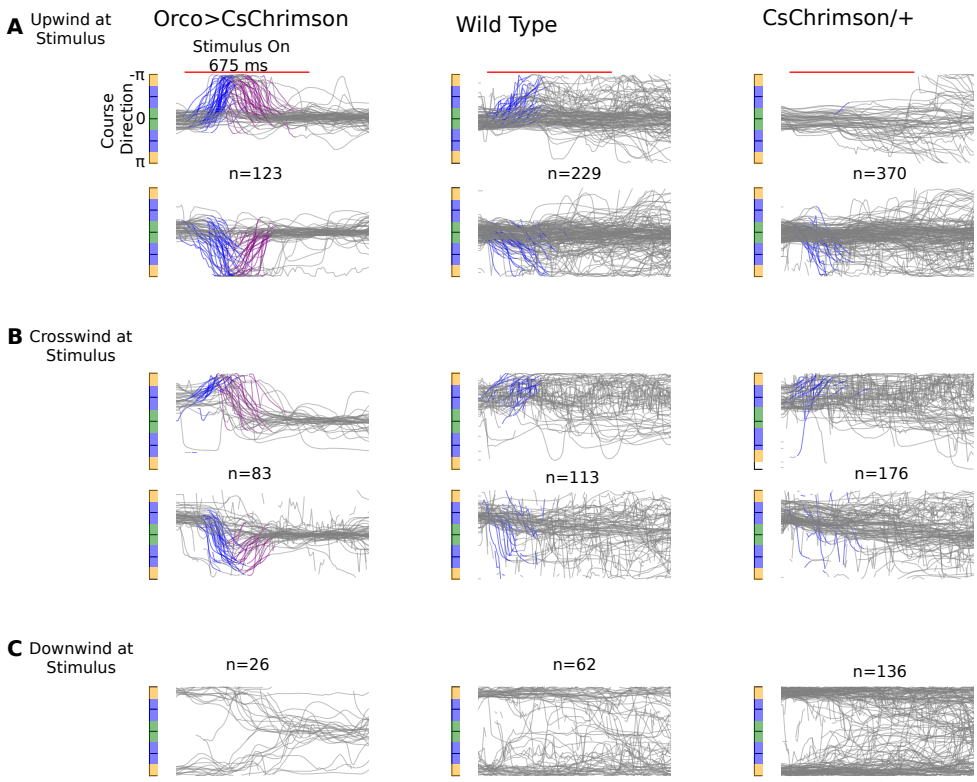

Supplementary Figure S8. Course changes after light flash are not a visual startle response. Direction vs. time plots for Orco>CsChrimson flies, wild-type flies, and CsChrimson/+ heterozygotes which received a flash event. Flies are separated into those oriented **A)** upwind at the time of the stimulus, **B)** crosswind at the time of the stimulus, or **C** downwind at the time of the stimulus. For wild-type and CsChrimson/+ flies, blue regions include trajectories that were sufficiently large to qualify as an ”anemometric” turn in our analysis. Downwind oriented flies are only shown in gray.

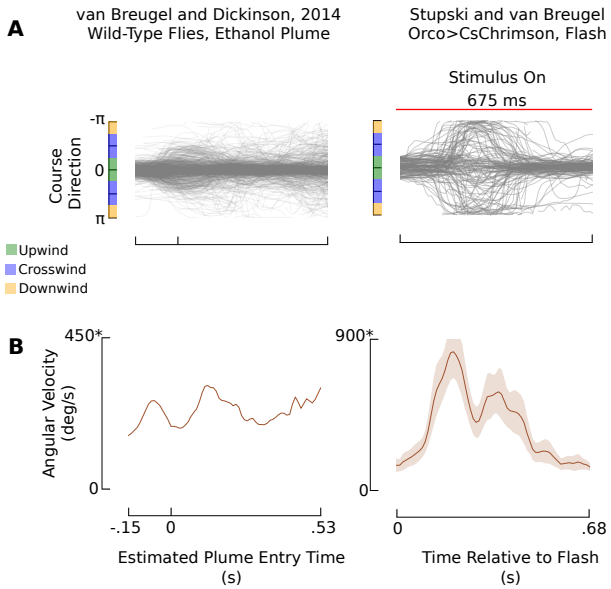

Supplementary Figure S9. Upwind-oriented flies often perform two-turns after encountering an ethanol plume. **A)** Left, course direction vs. estimated time of ethanol plume entry, data from [van Breugel and Dickinson, 2014], n=771. Right, Orco>CsChrimson flies which received a flash event, n=123, repeated from Fig. 6C. **B)** Angular velocity vs. time for flies encountering an ethanol plume (left) and Orco>CsChrimson flies receiving a flash (right). Note that angular velocities are not plotted to the same scale. Our reanalysis of the data from [van Breugel and Dickinson, 2014] suggests that the true estimated plume entry time may have been $\sim$ 150 ms prior to the originally estimated plume entry time.